

This discussion paper is/has been under review for the journal Solid Earth (SE).
Please refer to the corresponding final paper in SE if available.

Seismo-electrics, electro-seismics, and seismo-magnetics for earth sciences

L. Jouniaux¹ and F. Zyserman²

¹Institut de Physique du Globe de Strasbourg, CNRS and Université de Strasbourg UMR7516, Strasbourg, France

²CONICET and Facultad de Ciencias Astronómicas y Geofísicas, Universidad Nacional de La Plata, La Plata, Argentina

Received: 15 July 2015 – Accepted: 24 July 2015 – Published: 18 September 2015

Correspondence to: L. Jouniaux (l.jouniaux@unistra.fr)

Published by Copernicus Publications on behalf of the European Geosciences Union.

2563

Abstract

The seismo-electromagnetic method (SEM) is used for non-invasive subsurface exploration. It shows interesting results for detecting fluids such as water, ice, oil, gas, CO₂, and also to better characterise the subsurface in terms of porosity, permeability, and fractures. However, a limitation of this method is the low level of the induced signals. We first describe SEM's theoretical background, and the role of some key parameters. We then detail recent studies on SEM, through theoretical and numerical developments, and through field and laboratory observations, to show that this method can bring advantages compared to classical geophysical methods.

1 Introduction

Current methods of subsurface exploration are based on either seismic or electrical geophysical principles. The seismo-electromagnetic method combines both approaches, with the resolution of the seismics and the sensitivity of the electric methods to the fluids. It offers a non-invasive structure characterisation of the near surface earth from first few hundred metres up to several thousand metres depth, in terms of fluids (water, ice, oil, gas). Therefore it is a method supporting the management of water, oil and gas resources, specially the study of hydraulic and hydrocarbon reservoirs, of geothermal or fractured reservoirs, the resource prospection in glaciated regions, and CO₂ storage. SEM may characterise not only the depth and the geometry of the reservoir (Fig. 1 from Thompson et al., 2007), but also the fluid content. This method consists in observing electromagnetic signals induced through relative motion between rock and fluid, due to a propagating seismic wave. Seismo-electrics (SE) involves generating a seismic wave and measuring the electrical field contained within or generated by it (Fig. 2 from Thompson et al., 2005), while electroseismics (ES) does the opposite by injecting a large amount of current into the ground and measuring the resulting seismic energy. The relative motion between the fluid and the rock matrix is called elec-

2564

trokinetic phenomenon. In a porous medium the electric current density, linked to the ions within the fluid, is coupled to the fluid flow (Overbeek, 1952) so that the streaming potentials are generated by fluids moving through porous media (Jouniaux et al., 2009).

- 5 Two kinds of seismo-electromagnetic conversions are distinguished: (1) the first one is called the coseismic conversion, when the electric field is contained within the seismic wave and travels at its same speed, (2) the second kind is called the interface (IR) conversion, when a seismic wave encounters a boundary in physical properties between two media and travels at the velocity of the electromagnetic wave in the medium.
- 10 This electromagnetic wave can be received synchronously at multi-locations.

The second kind of conversion can be used to detect contrasts in permeability in the crust. A seismic source induces a seismic wave propagation downward up to the interface (Fig. 3). Because of the difference in the physical properties there is a charge imbalance that causes a charge separation on both sides of the interface. This acts

15 as an electric dipole which emits an electromagnetic wave that travels with the speed of the light in the medium and that can be detected at the surface (Fig. 4). The characteristic of this interfacial response is a flat event with a reversed polarity at either side of the source. The velocity of the seismic wave propagation is deduced by surface measurements of the soil velocity. Then the depth of the interface can be deduced by

20 picking the time arrival of the electromagnetic wave. Usually the seismoelectric signals show low amplitudes from 100 μ V to mV and suffer from low signal-to-noise ratio. Then signal processing needs filtering techniques such as those described in Butler and Russell (1993).

This method works advantageously in detecting zones of high fluid mobility and contrasts of physical parameters as porosity, geochemical fluids, permeability at depths

25 from few meters to few hundreds of meters (Thompson et al., 2005; Dupuis and Butler, 2006; Dupuis et al., 2007, 2009; Strahser et al., 2007, 2011; Haines et al., 2007a, b); for the characterization of permeable zones along a borehole (Mikhailov et al., 2000) and the groundwater exploration in a fractured rock aquifer (Fourie and Botha, 2001;

2565

Fourie et al., 2000). However surface observations are difficult to use for the exploration of deep formations because of the low efficiency of the seismo-electric conversion and the attenuation within the formations.

- Some field studies developed vertical seismoelectric profiles having a seismic source
- 5 below the studied interface allowing for the separation of the IR from the coseismic signal (Russell et al., 1997). Borehole investigations could also detect the location of opened fractures (Hunt and Worthington, 2000), and showed that the electric noise level was reduced at depth (Dupuis et al., 2009).

Previous reviews described the electrokinetics for geophysics (Beamish and Peart,

10 1998), the seismoelectric monitoring of producing oilfields (Gharibi et al., 2003), the Russian and Israeli experiments (Neishtadt et al., 2006), the frequency-dependence of streaming potential (Jouniaux and Bordes, 2012), and provide a tutorial on electrokinetics (Jouniaux and Ishido, 2012).

2 History

- 15 Seismoelectric techniques are based on electrokinetic coupling, largely studied in colloid and surface science. In Earth sciences, the seismoelectric IR was first reported by Ivanov (1939) and was called the effect of second kind or E-effect. Ivanov (1939) proposed that this effect can be induced by the streaming potential phenomenon in the moist soil. The first theoretical study on seismoelectric effect was published in 1944
- 20 by a Russian scientist (Frenkel, 1944). The Frenkel paper was re-published in 2005 as an historical outstanding contribution (Frenkel, 2005), while the propagation of seismic waves in a porous medium saturated with a viscous fluid is described by a theory developed by Biot (1956a, b). According to this theory the propagating waves are two dilatational waves and one rotational wave. Two kinds of dilatational waves are distinguished: the first kind corresponds to the solid and fluid moving in phase; the second
- 25 kind corresponds to the solid and fluid moving out of phase. The latter propagates at a lower velocity than the former, and is referred to as the Biot slow wave. In the seis-

2566

mic frequency range these slow waves are dissipative and die out rapidly with distance from the source.

The streaming potential was observed by Quincke (1861), as the reverse of the electro-osmosis phenomenon first observed by Wiedemann (1852) and Reuss (1809). The origin of this phenomenon was explained through the existence of an electric double layer acting as a condenser (von Helmholtz, 1879; Briggs, 1928). And anomalous behaviour of the zeta-potential in dilute solutions or in small capillaries had already been explained by the effect of surface conductance by McBain et al. (1929); Urban and White (1932); Rutgers (1940), and White et al. (1941).

First attempts on the seismic-electric effect were actually seismo-electric measurements when an electric current is injected through the earth. The observed effect was thought to be due to changes in the resistivity of the earth under the influence of seismic waves. A first explanation was proposed to be linked to the fluctuations in the current through the electrolytic cell because of variations of the electro-chemical conditions at the surface of the electrodes, induced by the mechanical vibrations (Thyssen et al., 1937). Then different experimental set-ups could eliminate the effect of electrode surface (Thompson, 1939); and later on Butler et al. (1996) showed that the resistivity modulation was not the relevant mechanism of the observed seismoelectric signals.

Martner and Sparks (1959) reported field measurements showing an IR generated at the base of a weathered layer, characterized by a change in seismic velocity, but not always associated with the top of the water table. Long and Rivers (1975) measured the electrical conductivity variations induced by seismic excitation. The measured electric signal, of 100 to 300 μV (per mm s^{-1}), correlated most strongly with the Rayleigh waves. However the estimate of resistivity change was only 0.015 %. So that the authors concluded that although the physical processes generating the signal was not elucidated, they were undoubtedly related to the condition of water in the pore spaces and the state of stresses. Russell et al. (1997) measured also an IR signal generated at a boundary between fill and glacial till at about 3 m depth using a seismic source in borehole below this boundary, at 5.5 m depth (at Haney, Canada). The

2567

seismoelectric data showed higher frequency than the seismic one, attributed to the fact that the seismoelectric wave is propagating with much less attenuation. These authors also characterized the seismoelectric signals induced in a zinc-rich orebody at the Lynx mine (British Columbia, Canada), and interpreted as due to microfracturing.

The electromagnetic field was measured using a device recording up to frequencies as high as 5 MHz. They showed high frequency content of the signals with oscillations at 1.3 MHz. It was concluded that these results were consistent with results from Russian researchers proposing that each type of ore/mineral has distinctive spectral peaks.

In the 1970s, laboratory experiments were performed to better understand the effect of salinity, of moisture, of porosity, and of frequency on the coseismic signal (Parkhomenko and Tsze-San, 1964; Parkhomenko and Gaskarov, 1971; Gaskarov and Parkhomenko, 1974; Migunov and Kokorev, 1977), which are detailed below and compared to more recent studies.

The generalization of Biot Theory including the electrokinetic effects was described by Neev and Yeatts (1989), based on the coupling equations of Onsager (1931).

At the same time in 1993/94 successful field experiments of seismoelectric conversion detected from an interface gas–water at depth of 300 m were published by Thompson and Gist (1993), and the theory for the coupled electromagnetics and acoustics of porous media was developed by Pride (1994). Later, the Pride's study was extended by including in the equations the effects of anisotropy, by Pride and Haartsen (1996). These works lead to further developments in this method.

3 Theoretical background

We present in this section the coupling equations derived from the Biot's theory and the Maxwell's equations; then we detail further developments on the equivalent electric dipole, and on the transfer function between seismic and electromagnetic energy.

2568

3.1 Frequency-dependence electrokinetics

The electrokinetic effect is due to fluid flow in porous media because of the presence of ions within the fluid which can induce electric currents when water flows. The general equation coupling the different flows is:

$$\mathbf{J}_i = \sum_{j=1}^N \mathcal{L}_{ij} \mathbf{X}_j \quad (1)$$

which links the forces \mathbf{X}_j to the macroscopic fluxes \mathbf{J}_i , through transport coupling coefficients \mathcal{L}_{ij} (Onsager, 1931).

Considering the coupling between the hydraulic flow and the electric flow, assuming a constant temperature, and no concentration gradients, the electric current density \mathbf{J}_e [A m⁻²] can be written as the following coupled equation:

$$\mathbf{J}_e = -\sigma_0 \nabla V - \mathcal{L}_{ek} \nabla P, \quad (2)$$

where P is the pressure that drives the flow [Pa], V is the electrical potential [V], σ_0 is the bulk electrical conductivity [S m⁻¹], \mathcal{L}_{ek} the electrokinetic coupling [A Pa⁻¹ m⁻¹]. Thus the first term in Eq. (2) is the Ohm's law. The coupling coefficients must satisfy the Onsager's reciprocal relation in the steady state. This reciprocity has been verified on porous materials (Miller, 1960; Auriault and Strzelecki, 1981) and on other natural materials (Beddiar et al., 2002).

When the electrokinetic effect is induced by seismic wave propagation, which leads to a relative motion between the fluid and the rock matrix, the electrokinetic coefficient depends on the frequency ω as the dynamic permeability $k(\omega)$ (Smeulders et al., 1992). The theory for the coupled electromagnetics and acoustics of porous media was developed by Pride (1994). The transport relations (Pride, 1994, Eqs. 250 and

2569

251) are:

$$\mathbf{J}_e = \sigma(\omega) \mathbf{E} + \mathcal{L}_{ek}(\omega) (-\nabla P + \omega^2 \rho_f \mathbf{u}_s), \quad (3)$$

$$-i\omega \mathbf{J}_f = \mathcal{L}_{ek}(\omega) \mathbf{E} + \frac{k(\omega)}{\eta_f} (-\nabla P + \omega^2 \rho_f \mathbf{u}_s). \quad (4)$$

The electrical fields and mechanical forces which induce the electric current density \mathbf{J}_e and the fluid flow \mathbf{J}_f are, respectively, \mathbf{E} and $(-\nabla P + i\omega^2 \rho_f \mathbf{u}_s)$, where P is the pore-fluid pressure, \mathbf{u}_s is the solid displacement, \mathbf{E} is the electric field, ρ_f is the pore-fluid density, η_f the dynamic viscosity of the fluid [Pa s], and ω is the angular frequency.

The electrokinetic coupling $\mathcal{L}_{ek}(\omega)$ describes the coupling between the seismic and electromagnetic fields and is complex and frequency-dependent (Pride, 1994; Reppert et al., 2001):

$$\mathcal{L}_{ek}(\omega) = \mathcal{L}_{ek} \left[1 - i \frac{\omega}{\omega_c} \frac{m}{4} \left(1 - 2 \frac{d}{\Lambda} \right)^2 \left(1 - i^{3/2} d \sqrt{\frac{\omega \rho_f}{\eta}} \right)^2 \right]^{-\frac{1}{2}}, \quad (5)$$

where m and Λ are geometrical parameters of the pores (Λ is defined in Johnson et al. (1987) and m is in the range 4–8), d the Debye length. The electrokinetic coupling is an important parameter: if this coupling is null, then there is no seismo-electric nor electro-seismic conversion. The transition frequency ω_c defined in the Biot's theory separates the viscous and inertial flow domains and depends on the intrinsic permeability k_0 [m²]. The transition angular frequency ω_c is defined as:

$$\omega_c = \frac{\phi \eta}{\alpha_\infty k_0 \rho_f}, \quad (6)$$

where ϕ is the porosity, α_∞ is the tortuosity.

2570

The electrokinetic coupling can not be directly quantified in the laboratory, whereas it is possible to measure the streaming potential C_{s0} induced by a pressure gradient. Both are related through

$$\mathcal{L}_{ek}(\omega) = -\sigma_0 C_{s0}(\omega); \quad (7)$$

So the frequency-dependence of the streaming potential coefficient has been studied (Packard, 1953; Cooke, 1955; Groves and Sears, 1975; Sears and Groves, 1978; Chandler, 1981; Reppert et al., 2001; Schoemaker et al., 2007, 2008) mainly on synthetic samples, and recently on sand (Tardif et al., 2011), and on unconsolidated materials (Glover et al., 2012). In 1953 Packard (1953) proposed a model for the frequency-dependent streaming potential coefficient for capillary tubes, assuming that the Debye length is negligible compared to the capillary radius, based on the Navier–Stokes equation:

$$C_{s0}(\omega) = \frac{\Delta V(\omega)}{\Delta P(\omega)} = \left(\frac{\epsilon \zeta}{\eta \sigma_f} \right) \left(\frac{2}{a \sqrt{\frac{i\omega \rho_f}{\eta}}} \frac{J_1 \left(a \sqrt{\frac{i\omega \rho_f}{\eta}} \right)}{J_0 \left(a \sqrt{\frac{i\omega \rho_f}{\eta}} \right)} e^{-i\omega t} \right); \quad (8)$$

where ω is the angular frequency, a is the capillary radius, J_1 and J_0 are the Bessel functions of the first order and the zeroth order, respectively, and ρ_f is the fluid density, and the transition angular frequency for a capillary is:

$$\omega_c = \frac{\eta}{\rho_f a^2}. \quad (9)$$

The absolute magnitude of the streaming potential coefficient normalized by the steady-state value was calculated by Packard (1953) as:

$$f(Y_a) = \left(\frac{-2}{Y_a} \frac{i \sqrt{i} J_1(\sqrt{i} Y_a)}{J_0(\sqrt{i} Y_a)} e^{-i\omega t} \right), \quad (10)$$

2571

which is equal to Eq. (8), but expressed as a function of the parameter $Y_a = a \sqrt{\frac{\omega \rho_f}{\eta}}$, the transition frequency being obtained for $Y_a = 1$. The real part and the imaginary part of the theoretical Packard's streaming potential coefficient (Eq. 8) was calculated for different capillary radii by Reppert et al. (2001) (Fig. 5). It can be seen that the larger the radius, the lower the transition frequency, as shown above by the different theories. The streaming potential coefficient is constant up to the transition angular frequency, and then decreases with increasing frequency.

In 2001, Reppert et al. (2001) used the low- and high-frequency approximations of the Bessel functions to propose the following formula, which corresponds to their Eq. (26) corrected with the right exponents -2 and $-1/2$:

$$C_{s0}(\omega) = \left(\frac{\epsilon \zeta}{\eta \sigma_f} \right) \left[1 + \left(\frac{-2}{a} \sqrt{\frac{\eta}{\omega \rho_f}} \left(\frac{1}{\sqrt{2}} - \frac{1}{\sqrt{2}} i \right) \right)^{-2} \right]^{-\frac{1}{2}}, \quad (11)$$

with the transition angular frequency

$$\omega_c = \frac{8\eta}{\rho_f a^2}, \quad (12)$$

and showed that this model was not very different from the model proposed by Packard (1953).

More recently, Walker and Glover (2010) proposed a simplified equation of Pride's development assuming that the Debye length is negligible compared to the characteristic pore size, and assuming the parameter:

$$m = 8 \left(\frac{\Lambda}{r_{eff}} \right)^2, \quad (13)$$

leading to the equation:

$$\mathcal{L}_{\text{ek}}(\omega) = \mathcal{L}_{\text{ek}} \left[1 - 2i \frac{\omega}{\omega_c} \left(\frac{\Lambda}{r_{\text{eff}}} \right)^2 \right]^{-\frac{1}{2}}, \quad (14)$$

with r_{eff} the effective pore radius, and a transition angular frequency

$$\omega_c = \frac{8\eta}{\rho_f r_{\text{eff}}^2}. \quad (15)$$

- 5 More details on the frequency-dependent streaming potentials are provided by the review of Jouniaux and Bordes (2012) including a description of different experimental apparatus.

3.2 Theoretical developments

10 The mechanisms involved in the subsurface electrokinetic coupling have been summarized by Beamish (1999) in Fig. 6. The first mechanism occurs in the first Fresnel-zone, when a spherical P wave traverses an interface directly beneath the source: this is the IR providing instantaneous arrivals across arrays of surface dipoles. This mechanism occurs at interfaces between different streaming potential coefficients. The second mechanism is related to the refracted-head wave travelling along the interface, 15 which generates an electromagnetic field providing time-dependent arrivals at arrays of surface dipoles. This mechanism occurs at interfaces with a difference in both acoustic and electrokinetic properties. The third mechanism is linked to surface waves, including the direct (compressional) wave and the surface/Rayleigh wave, travelling along the ground surface.

- 20 The electromagnetic field induced by an interface excited by a seismic pulse can be approximated to an electric dipole located directly under the source (Thompson and Gist, 1993). Indeed a spherical seismic wave incident on a horizontal interface

2573

induces circular regions, called the Fresnel zones, of positive and negative displacement moving outward along the interface. The first Fresnel zone is the part of the horizontal interface reached by the seismic wave within one-half wavelength from the initial arrival, successive Fresnel zones being excited at later times. So that a number 5 of electric dipoles are finally excited. As the electric field falls off with distance r as $1/r^3$ for a dipole and $1/r^5$ for an octupole, the electric field from higher-order Fresnel zone can be neglected compared to the one of the first Fresnel zone (Thompson and Gist, 1993). Moreover Thompson and Gist (1993) calculated a signal-to-noise ratio for the maximum of the IR of still about 50 for an interface gas–water at 300 m depth, for 10 a seismic pulse center frequency of 50 Hz.

Garambois and Dietrich (2001) calculated the electric field radiated by two interfaces at 2 m depth and 10 m depth, by summing the individual contributions of all dipoles contained within the Fresnel zones, which are circular surfaces of radii 3.75 and 7.07 m for depths of the interface of 2 and 10 m respectively. The results show that the horizontal electric field has a dipolar property with a change of polarity on opposite sides 15 of the shotpoint. Moreover the maximum of the horizontal electric field decreases as the depth of the interface increases (Fig. 7).

Fourie and Botha (2001) noticed that the first Fresnel zone is large, so that the recorded signal will include the lateral variations of the interface on about 40 m distance 20 from its center, for an interface at 50 m depth. The ES Fresnel zones are larger than the seismic Fresnel zone, twice as large for interfaces at depths much greater than the dominant wavelength, because only the one-way distance to the interface is important, the EM wave propagating several orders of magnitude faster than the seismic waves (Fourie, 2006). By modelling an interface consisting in ring-shaped zone between two 25 media of different seismic velocities, Fourie and Botha (2001) calculated the horizontal electric field at a short distance from the seismic source (0.5 m). The authors showed that the amplitude of the electric field is decreasing for increasing inactive distance (the inner radius of the ring-shaped zone). They showed that when the source is a Ricker wavelet, the maximum of the electric field occurs for an inactive zone of 4 m radius

(for an interface at 40 m depth), rather than for a full active ring-shaped zone. But this maximum was only about 1 % greater than the electric field calculated for the full active ring-shaped zone. So that the assumption that the IR signal is generated at a position vertically below the seismic source is rather valid. However the lateral resolution of surface seismo-electric measurements will remain weaker than for seismics.

Dupuis et al. (2009) proposed a near field analysis of the spatial and temporal variations of the polarity and amplitude of the seismoelectric conversions observed in boreholes. They noted that the lateral extent of the seismic source at the interface is the Fresnel radius, while the vertical extent is the dominant wavelength of the compressional seismic wave. Therefore, if the electric dipoles are short in comparison to the height of the source zone, it is possible to measure the signal within this zone, which has a reverse polarity of the signal observed above and below the source zone.

The ability of the seismoelectric method to detect thin embedded layers depends on the constructive and destructive interferences of the signal induced at its bottom and its top interfaces. The seismoelectric response from a thin fluid-saturated layer may be enhanced by the constructive interferences (Haartsen and Pride, 1997). The embedded layer needs to be thicker than half the dominant wavelength to be resolvable. Fourie (2006) showed that for both fast and slow waves (corresponding to a wavelength of about 29 and 0.8 m respectively), beds with thicknesses less than one quarter of the wavelength, result in a total response weaker than the response from the upper interface alone.

The transfer functions between the coseismic electric field, the coseismic magnetic field, and the acceleration and displacement, have been also theoretically derived, in an isotropic and homogeneous wholespace (Pride and Haartsen, 1996), considering a plane-wave solution of the governing equations.

The two main cases first considered are the relation between the electric field and the displacement for the compressional waves and the relation between the magnetic field and the displacement for shear waves. The other combinations are small or zero. Indeed the electric field associated with transverse waves does not result from a charge

2575

separation, but it is induced by the induction of the magnetic field and has a small amplitude. For the transverse mode two different polarizations exist: the SH-TE case corresponds to SH-shear waves and to a transverse electric field of EM waves that are both horizontally polarized in the cross-line direction; the SV-TM case, on the other hand, consists of vertically polarized SV shear waves and a horizontally polarized transverse magnetic field of EM waves.

Moreover there is no magnetic field associated to compressional waves (Garambois and Dietrich, 2001).

Garambois and Dietrich (2001) studied the low frequency assumption valid at seismic frequencies, meaning at frequencies lower than the Biot's frequency separating viscous and inertial flows and gave the coseismic transfer function for low frequency longitudinal plane waves. In this case, and assuming the Biot's moduli $C \ll H$, they showed that the seismoelectric field \mathbf{E} is proportional to the grain acceleration for longitudinal fast P waves:

$$\mathbf{E} \simeq -\frac{\mathcal{L}_{ek}}{\sigma_0} \rho_f \ddot{\mathbf{u}} = \frac{\epsilon_f \zeta}{\eta \sigma_f} \rho_f \ddot{\mathbf{u}}. \quad (16)$$

Equation (16) shows that transient seismo-electric magnitudes will be affected by the density of the fluid, the water conductivity and the zeta potential (which depends on the water pH), the dielectric constant and viscosity of the fluid.

These authors also showed that the magnetic field is proportional to the grain velocity for displacements associated to transverse SH and SV waves as:

$$|\mathbf{H}| \simeq \frac{1}{F} \frac{\epsilon_f |\zeta|}{\eta} \rho_f \sqrt{\frac{G}{\rho}} |\dot{\mathbf{u}}|. \quad (17)$$

In Eq. (17), G is the shear modulus of the framework and ρ the bulk density.

The definitions of the C and H moduli are those of Biot (1962). Therefore the magnetic field depends also on the density of the fluid, the zeta potential (which depends

2576

on the water pH), the dielectric constant and viscosity of the fluid, but also on the shear modulus of the framework, the bulk density and the formation factor, so indirectly on the permeability.

Recently Bordes et al. (2015) derived the transfer functions ψ for the seismoelectric field, neglecting the Biot slow waves, in the dynamic domain (as a function of frequency), associated both to compressional P waves and shear S waves:

$$\mathbf{E}(\omega) = \psi_{p\text{-dyn}} \ddot{\mathbf{u}}_p(\omega) + \psi_{s\text{-dyn}} \ddot{\mathbf{u}}_s(\omega). \quad (18)$$

For the low frequency assumption, the authors showed that

$$\mathbf{E}(\omega) = -C_{s0} \rho_f \left[\left(1 - \frac{\rho}{\rho_f} \frac{C}{H} \right) \ddot{\mathbf{u}}_p(\omega) - i \frac{\mu}{\omega} \frac{G}{\rho} \frac{\phi}{\alpha_\infty} \sigma_f \ddot{\mathbf{u}}_s(\omega) \right]. \quad (19)$$

Following the approach of Warden et al. (2013), by introducing the effective fluid model into the Pride's theory, and replacing C_{s0} by $C_{s0}(S_w)$, the authors generalized the transfer function formulation for unsaturated conditions. They tested different models of the streaming potential water-content dependency and plotted the results of the dynamic transfer function of the electric field as a function of water saturation (Fig. 8). It is shown that the transfer function is not monotonously decreasing with decreasing water content, but first increases with decreasing water saturation, up to a saturation between 0.9 and 0.5, according to the different hypotheses of frequency-domain and saturation dependency of the SPC. Note that even the SPC is decreasing monotonously with decreasing saturation (case of model from Guichet et al., 2003, for example), the transfer function still shows a non-monotonous behaviour.

4 Role of key parameters

We present here the role of key parameters such as the zeta potential, the formation factor, the permeability, the surface conductivity, the temperature, and the water-content, on the electrokinetic coupling.

2577

4.1 Role of key parameters on the steady-state electrokinetic coupling

The steady-state electrokinetic coupling is defined as:

$$\mathcal{L}_{ek} = -\sigma_0 C_{s0}, \quad (20)$$

where the streaming potential coefficient C_{s0} [V Pa^{-1}] is defined when the electric current density \mathbf{J}_e is zero. This streaming potential coefficient is related to the electric double layer. The electric double layer (Debye and Huckel, 1923) is made up of the Stern layer (Stern, 1924) where cations are adsorbed onto the surface, and the Gouy diffuse layer (Gouy, 1910) where the number of counterions exceeds the number of anions (Adamson, 1976; Davis et al., 1978; Hunter, 1981). The streaming current, due to the motion of the diffuse layer, is induced by a fluid pressure difference along the interface (second term in Eq. 2). This streaming current is then balanced by the conduction current (first term in Eq. 2), leading to the streaming potential V . More details on the electric double layer are provided in the tutorial of the special issue on electrokinetics in Earth Sciences by Jouniaux and Ishido (2012), with the description of the electric potential within the electric double layer.

The electric current density can also be expressed as a function of the volumetric charge density Q_v and the Darcy velocity v . The volumetric charge density is sometimes expressed as a function of permeability, but this formula has not been validated using independent measurements of permeability and charge density deduced from CEC measurements. Usually the volumetric charge density is deduced from streaming potential coefficient measurements using the following formula:

$$Q_v = -\frac{C_{s0} \sigma_0}{K}, \quad (21)$$

with K the hydraulic conductivity (in m s^{-1}), leading to a dependence between Q_v and permeability, which does not prove by itself the existence a real link between both

quantities. Therefore this approach is considered not appropriate and should not be used.

When the surface conductivity can be neglected compared to the fluid conductivity, and assuming a laminar fluid flow and identical hydraulic and electric tortuosity, the streaming coefficient is described by the well-known Helmholtz–Smoluchowski equation (Dukhin and Derjaguin, 1974):

$$C_{s0} = \frac{\epsilon_f \zeta}{\eta_f \sigma_f}. \quad (22)$$

The influencing parameters on this streaming potential coefficient are therefore the dielectric constant of the fluid ϵ_f , the viscosity of the fluid η_f , the fluid conductivity σ_f and the zeta potential ζ .

4.1.1 Effect of zeta potential

The zeta potential is defined as the electric potential at the slipping plane within the electric double layer. The zeta potential itself depends on rock, fluid composition, and pH (Ishido and Mizutani, 1981; Jouniaux et al., 1994, 2000; Jouniaux and Pozzi, 1995; Lorne et al., 1999; Guichet et al., 2006; Mainault et al., 2006; Jaafar et al., 2009; Vinogradov et al., 2010).

The charge density at the surface of the minerals results from surface complexation reactions. The quartz surface can be modelled with silanol $>SiOH$ group (Davis et al., 1978). The potential-determining ions OH^- and H^+ are adsorbed onto the surface of the mineral and determine the charge density on the inner plane. The surface charge is therefore dependent on the pH.

There exists a pH for which the total surface charge is zero: this is the point of zero charge and this pH is called pH_{pzc} (Davis and Kent, 1990; Sposito, 1989). In this case this electrokinetic effect is zero. The charge is positive for $pH < pH_{pzc}$ and negative for $pH > pH_{pzc}$. The pH_{pzc} for quartz is in the range $2 < pH_{pzc} < 4$ (Parks, 1965; Lorne et al., 1999). The calcite surface can be modelled with $>CaOH$ and $>CO_3H$ groups.

2579

Carbonate ions and Ca^{2+} are the determining-potential ions. The electrokinetic behaviour on carbonates is more complicated. The pH_{pzc} varies from 7 to 10.8 according to the authors (VanCappellen et al., 1993). It is possible to model simple interfaces and to calculate the zeta potential in simple cases (Guichet et al., 2006). This modeling can be performed assuming the triple-layer-model (TLM) which distinguishes three planes to describe the electric double layer: the inner Helmholtz plane for counter ions directly bound to the mineral (assumed to be chemically adsorbed), the outer Helmholtz plane for weakly bound counter ions (assumed to be physically adsorbed), and a d' plane associated with the smallest distance between the mineral surface and the counter ions in the diffuse layer. It has been proposed that the slipping plane lies near the distance of closest approach of dissociated ions and that the ζ potential can be calculated as the potential on this plane (Davis and Kent, 1990).

At a given pH the most influencing parameter on the streaming potential coefficient is the fluid conductivity. It has been proposed that $C_{s0} = -1.2 \times 10^{-8} \sigma_f^{-1}$ (Allègre et al., 2010), based on data collected in the literature on sandstones and sands (Fig. 9), which leads to a zeta potential equal to -17 mV assuming Eq. (22) and that zeta potential, dielectric constant, and viscosity do not depend on fluid conductivity. These assumptions are not exact, but the value of zeta is needed for numerous modellings which usually assume the dielectric constant and viscosity independent of the fluid conductivity. Therefore an average value of -17 mV for such modellings is fairly exact, at least for media with no clay nor calcite, and in the fluid conductivity range excepting very high values. Another formula is often used (Pride and Morgan, 1991) based on quartz minerals rather than on sands and sandstones, which may be less appropriate for field applications.

4.1.2 Effect of formation factor and permeability

Note that assuming the Helmholtz–Smoluchowski equation for the streaming potential coefficient leads to the steady-state electrokinetic coupling inversely dependent on the

formation factor F as:

$$\mathcal{L}_{\text{ek}} = \frac{\epsilon_f \zeta}{\eta_f F}. \quad (23)$$

Therefore the steady-state electrokinetic coupling does not depend directly on the fluid conductivity. It can depend indirectly on the fluid conductivity only if the zeta potential is assumed to vary with the fluid salinity. This electrokinetic coupling still depends on the dielectric constant of the fluid ϵ_f , the viscosity of the fluid η_f , and the ζ potential itself depending on the pH. Moreover it depends on the formation factor which is related to the compaction of the rock. Indeed the formation factor is related to the porosity through

$$F = \phi^{-m}, \quad (24)$$

with m being Archie's cementation exponent (Archie, 1942).

The formation factor is inversely related to the permeability and proportional to the hydraulic radius R by $F = CR^2/k_0$ (Paterson, 1983) with C a geometrical constant usually in the range 0.3–0.5. Since the permeability can vary about fifteen orders of magnitude, whereas this is not the case of the hydraulic radius, the static electrokinetic coupling \mathcal{L}_{ek} will increase with increasing permeability. Note that we can read in the literature that the steady-state electrokinetic coupling is independent of permeability, which is not exact because porosity over tortuosity represents the formation factor, which is linked to the permeability.

Therefore any contrast in the following properties will induce a seismo-electric or electro-seismic conversion: contrast in the dielectric constant of the fluid, the viscosity of the fluid, the porosity, the formation factor, the permeability, and the ζ potential itself depending on the pH and possibly on the fluid conductivity.

2581

4.1.3 Effect of surface conductivity

When the surface conductivity can not be neglected, the streaming potential coefficient can be written as:

$$C_{s0} = \frac{\epsilon_f \zeta}{\eta_f (\sigma_f + \sigma_s)}, \quad (25)$$

with σ_s the surface conductivity (S m^{-1}) (Rutgers, 1940). It is difficult and time-consuming to determine experimentally the surface conductivity of one sample, because it needs measurements with different salinities including very low ones. Therefore this parameter is often deduced from $\sigma_s = 2\Sigma_s/R$, with Σ_s the surface conductance (S) and R the hydraulic radius of the rock or the pore radius (Rutgers, 1940; Alkafef and Alajmi, 2006; Wang and Hu, 2012). It has been shown that the surface conductivity in Fontainebleau sand is less than $2 \times 10^{-4} \text{ S m}^{-1}$ (Guichet et al., 2003). Typical values of the surface conductance for quartz or sandstone range from 8.9×10^{-9} to $4.2 \times 10^{-8} \text{ S}$ (Block and Harris, 2006) and $2.5 \times 10^{-9} \text{ S}$ for clays (Revil and Glover, 1998). The surface conductivity can neither be neglected in clay layers, nor when the hydraulic radius is of the order of the Debye length. This latter case can be encountered when the fluid is not very conductive, as below $2 \times 10^{-3} \text{ S m}^{-1}$ in sandstones (Pozzi and Jouniaux, 1994). In that case the streaming potential coefficient can be lowered compared to the expected value. Since the hydraulic radius can be indirectly connected to the permeability, the effect of surface conductivity can explain some observations of permeability-dependence of the streaming potential coefficient (Jouniaux and Pozzi, 1995).

The effect of surface conductivity can also be taken into account if the formation factor F is known, and if the rock conductivity σ_r , possibly with a surface component, is also known, as:

$$C_{s0} = \frac{\epsilon_f \zeta}{\eta_f \sigma_{\text{eff}}} = \frac{\epsilon_f \zeta}{\eta_f F \sigma_r}. \quad (26)$$

2582

The advantage of this approach is that neither the surface conductivity nor the conductance are directly needed.

4.1.4 Effect of temperature

The effect of temperature on the streaming potential has been studied both experimentally and theoretically. The streaming potential coefficient on quartz was measured to increase (in absolute value) from -2 to $-3 \times 10^{-6} \text{ V Pa}^{-1}$ between 20 and 70°C (with 10^{-3} KNO_3 at pH 6.1 at low temperature, and up to pH 4.2 at high temperature) (Ishido and Mizutani, 1981). The authors pointed out, from the equilibrium time needed for the measurements of the order of twenty to hundred and fifty hours, that the thermal equilibrium of charge distribution near the interface is not reached very quickly. On Westerly granite the streaming potential coefficient was measured to decrease (in absolute value) from -2.3 to about $-1.9 \times 10^{-7} \text{ V Pa}^{-1}$ between 5 and 70°C (with NaCl solution of resistivity $8.5 \Omega \text{ m}$ at 25°C) (Morgan et al., 1989). The differences between these two studies is that the last one was performed in four hours for the entire experiment, so that the silica equilibrium was not attained, although the authors mentioned that silica equilibrium takes many days to be established. Taking into account the effect of temperature on the permittivity, the conductivity, and the viscosity, the authors concluded that the zeta potential was constant in this range of temperature, and at this rate of measurements.

Reppert and Morgan (2003a) studied theoretically the effect of temperature on the different parameters of the streaming potential coefficient. They showed that the viscosity is the most dominant term in the temperature-dependent SPC. Then the fluid conductivity also shows a strong dependence on the temperature. The permittivity shows a small dependence on temperature. These effects can be balanced so that assuming a zeta potential constant and a temperature-dependence on the three other parameters, the SPC is roughly independent of the temperature (Reppert and Morgan, 2003a).

2583

However measurements of the SPC on sandstones and granite samples in the temperature range 20 – 200°C , allowing very long equilibrium times such as 700 – 1200 h , showed that the SPC is not constant (Reppert and Morgan, 2003b). The SPC is decreasing in magnitude from 20 to 160°C , from about 2×10^{-7} to $3 \times 10^{-8} \text{ V Pa}^{-1}$ (Fontainebleau sandstone) and from about 1×10^{-7} to $2 \times 10^{-8} \text{ V Pa}^{-1}$ (Berea sandstone), before increasing in magnitude up to 200° , up to $4 \times 10^{-8} \text{ V Pa}^{-1}$ (Fontainebleau sandstone) and $1 \times 10^{-7} \text{ V Pa}^{-1}$ (Berea sandstone) for temperatures up to 200°C . The fluid conductivity, initially $10^{-3} \text{ mol L}^{-1} \text{ NaCl}$, was increased from 0.01 to 0.13 S m^{-1} (for Fontainebleau sandstone). The observed SPC on Westerly granite, of the order of $5 \times 10^{-8} \text{ V Pa}^{-1}$, showed a reverse behaviour, increasing in magnitude up to 120°C , and then decreasing with increasing temperature. The interpretation in term of zeta potential behaviour as a function of temperature is very difficult because the pH of the electrolyte is changing with the temperature.

Further measurements of the SPC in the range 20 – 200°C were performed on Inada granite, and showed an increase in the SPC magnitude with increasing temperature, this increase being larger using low-concentration electrolyte (Tosha et al., 2003). When the sample is initially saturated by $10^{-3} \text{ mol L}^{-1} \text{ KCl}$ the SPC increases from 5×10^{-8} to $12 \times 10^{-8} \text{ V Pa}^{-1}$; when initially saturated by $10^{-2} \text{ mol L}^{-1} \text{ KCl}$ the SPC increases from 3×10^{-8} to about $7 \times 10^{-8} \text{ V Pa}^{-1}$; and when the sample is initially saturated by $10^{-1} \text{ mol L}^{-1} \text{ KCl}$ the SPC increases from 10^{-8} to $2.5 \times 10^{-8} \text{ V Pa}^{-1}$. Unfortunately the authors did not measure the fluid conductivity after equilibrium, and at the end of the temperature increase. But these results are coherent with those of Reppert and Morgan (2003b). The different behaviour of the SPC in sandstones and granite still needs further explanations, and is probably related to different behaviours in pH, surface charge density and dissociation constant in quartz–water or plagioclase/feldspar–water systems, as possible precipitation of secondary minerals.

Another experiment on quartz–Al–K–NO₃ system from Ishido and Mizutani (1981) showed that the magnitude of zeta potential first increases with temperature up to about 45°C and then decreases with increasing temperature up to 80°C . This behaviour was

2584

not understood until the study of Guichet et al. (2003). These authors showed that the solutions are oversaturated with aluminium, and that the precipitation of $\text{Al}(\text{OH})_3$ is expected. They showed that a Triple Layer Model (TLM) calculations for a gibbsite- KNO_3 system can account for these measurements. These authors concluded that the precipitation of a secondary mineral can hide the electrical properties of the primary rock, and that the interfacial processes of precipitation/dissolution should be taken into account when dealing with the temperature effect.

To interpret seismoelectric conversion in a geothermal context the first problem to resolve is the knowledge of the interfacial chemistry of the rock/water system, and to know which secondary minerals are present. Then a zeta potential value can be estimated according to the mineral/water system, and a SPC value deduced. Afterward the effect of temperature on SPC can be estimated based on observations performed on simple systems at fluid conductivity about 0.1 S m^{-1} , as quartz- or granite-water showing a decrease of a factor 5 to 7 of the SPC from 20 to 160°C (Berea and Fontainebleau sandstone, Reppert and Morgan, 2003b), or an increase of a factor three of the SPC from 20 to $120\text{--}200^\circ\text{C}$ (Westerly granite, Reppert and Morgan, 2003b; Inada granite, Tosha et al., 2003).

4.1.5 Effect of water-content

The effect of water-content has been studied on the streaming potential coefficient, but the conclusions are still discussed, mainly because of a possible effect of the flow. Perrier and Morat (2000) were the first to propose that the SPC depends on the relative permeability.

These authors proposed that the electrokinetic coefficient varies as a function of the relative permeability k_r as:

$$C_{s0}(S_w) = C_{\text{sat}} \frac{k_r(S_w)}{S_w^n}, \quad (27)$$

2585

with S_w the water saturation, and n the second Archie exponent (Archie, 1942). Revil et al. (2007) proposed a similar formula, assuming that the excess countercharge density scales inversely with water saturation.

Then Jackson (2010) developed a model for the electrokinetic coefficient for unsaturated conditions through a capillary tubes model, including water or oil as fluid. Jackson (2010) showed that the electrokinetic coefficient depends on the relative permeability, the relative charge density, and the fluid content, assuming that Archie's law is valid, as:

$$C_{s0}(S_w) = C_{\text{sat}} \frac{k_r(S_w)Q_r(S_w)}{S_w^n}, \quad (28)$$

with Q_r the relative excess charge density: $Q_r(S_w) = Q(S_w)/Q(S_w = 1)$. Jackson (2008, 2010) showed that the excess countercharge density does not scale inversely with water saturation, but it depends on the pore scale distribution of fluid and charge.

Finally, Allègre et al. (2012) modelled both Richards' equation for hydrodynamics and the Poisson's equation for electrical potential for unsaturated conditions using a 1-D finite element method. They concluded, based on laboratory experiments and using these equations, that the unsaturated electrokinetic coefficient should have a non-monotonous behaviour:

$$C_{s0} = C_{\text{sat}} S_e [1 + \beta(1 - S_e)^\gamma], \quad (29)$$

where the effective saturation is:

$$S_e = \frac{S_w - S_{wr}}{1 - S_{wr}}, \quad (30)$$

and β and γ are two adjusted parameters, β depending on the initial flow conditions, particularly on the water velocity at the beginning of the drainage phase. A non-monotonous behavior is supported by the observations of Allègre et al. (2010) and also

2586

by the observations of Revil et al. (2007) and Revil and Cerepi (2004) as detailed in Allègre et al. (2011). Recently Allègre et al. (2015) showed that the interface between water and air should also be taken into account, since this interface is negatively charged, as the interface between the rock matrix and the water. Moreover during a drainage the amount of this interface does not decrease with decreasing water-saturation, but first increases before decreasing, leading to a non-monotonic behaviour of the resulting SPC (Allègre et al., 2015).

The Table 1 summarises the ratios $C_{s0}(S_w)/C_{sat}$ proposed by different authors.

4.2 Role of key parameters on the transition frequency

The transition angular frequency separating viscous and inertial flows in a porous medium can be rewritten by inserting $\alpha_\infty = \phi F$ with F the formation factor that can be deduced from resistivity measurements using Archie's law, as:

$$\omega_c = \frac{1}{F} \frac{\eta}{k_0 \rho_f}. \quad (31)$$

It can be also re-written as a function of the hydraulic radius R as

$$\omega_c = \frac{\eta}{\rho_f C R^2}. \quad (32)$$

The Eq. (32) shows that the transition angular frequency in a porous medium is inversely proportional to the square of the hydraulic radius.

It has also been shown by Jouniaux and Bordes (2012) that the transition frequency $f_c = \omega_c/2\pi$ is inversely proportional to the permeability as:

$$\log_{10}(f_c) = -0.78 \log_{10}(k) - 5.5, \quad (33)$$

and varies from about 100 MHz for $k = 10^{-17} \text{ m}^2$ to about 10 Hz for $k = 10^{-8} \text{ m}^2$, so by seven orders of magnitude for nine orders of magnitude in permeability (Fig. 10).

2587

Therefore the transition angular frequency depends on the fluid viscosity, the fluid density, and on both the permeability and the formation factor. Although the permeability and formation factor are not independent factors it has been shown that the transition frequency is inversely proportional to the permeability.

5 Modelling and processing

The methods used to numerically approximate solutions to the seismoelectric/electroseismic equations could be classified according to the extent of the employed source, which can be either finite or point sources (generating 3-D responses), or infinitely long ones (2-D responses). They can also be classified according to the used approximating methodology; according to this choice, most of the methods use either Green's functions formulations, or are different variations of the Generalized Reflection and Transmission Matrix method (GMRT), finite differences methods (FD) or finite element methods (FE).

Before we delve into the works corresponding to this description, we mention some different studies, like the works of White (2005), who used seismic ray theory to determine the linear dependence between the magnitude of the electroseismic or seismoelectric responses and the electrokinetic coupling coefficient; while White and Zhou (2006) used Ursin's formalism to model electroseismic conversions on homogeneous layered media within the frame of a unified treatment of electromagnetic, acoustic and elastic waves. Moreover seismoelectric reflection and transmission at fluid/porous medium interfaces were investigated by Schakel and Smeulders (2010) who developed the dispersion relation for seismoelectric wave propagation in poroelastic media. These authors proved by means of a sensitivity analysis that electrolyte concentration, viscosity, and permeability highly influence seismoelectric conversions.

5.1 3-D response of stratified media

In Pride and Haartsen (1996), the governing equations controlling the electroseismic wave propagation were presented for a general anisotropic and heterogeneous porous material; uniqueness, energy conservation and reciprocity were derived. Moreover, the authors derived Green's functions for the coupled poroelastic and electromagnetic problem for the solid and fluid displacements and the electric field, and obtained responses to a point source in an isotropic and homogeneous whole space. Gao and Hu (2010) extended this work by developing the Green's function for the magnetic field and by considering moment tensors as sources. In Haartsen et al. (1998), relative flow Green's functions were derived to investigate numerically the effect of porosity, permeability and fluid chemistry on dynamic streaming currents caused by point forces in homogeneous porous media. The authors showed that the induced streaming current diminishes with increasing salinity, that its dependence with porosity is different if it is generated by P waves or S waves and that its behaviour with respect to permeability is different for sources applied to the elastic frame than for volume-injection sources.

Haartsen and Pride (1997) produced numerical experiments featuring seismic and electromagnetic point sources on horizontally stratified media; they used a global matrix method to obtain their results. They showed that the governing equations can be decoupled in two modes, namely the SHTE mode, involving the seismic SH and transverse electric TE, and the PSVTM mode, linking the seismic P -SV modes with the transverse magnetic TM mode; they showed that the interface response was similar to the one of a vertical electric dipole situated right beneath the seismic source. In Mikhailov et al. (1997) this algorithm was employed to compare synthetic seismoelectric conversions generated at a top soil-glacial till interface with field data. Not only they were able to observe seismoelectric conversions on the field, but also the numerical simulations qualitatively reproduced the observations. In Hu and Gao (2011), an extension to this algorithm is performed including a moment tensor point source. In this way, electromagnetic fields induced by a finite fault rupture are studied. Their simula-

2589

tions showed that the rupturing fault generates observable permanent electromagnetic field disturbances; two types of electric field characters were observed: the coseismic oscillatory variation and the postseismic decaying variation. They also observed that when the fault rupturing stops and the seismic waves pass far away, the magnetic field vanishes while the electric field remains, decaying slowly and lasting for hundreds of seconds.

In a work mainly devoted to show seismoelectric field experiments, Garambois and Dietrich (2001) developed transfer functions and showed that the electric field accompanying the compressional waves is approximately proportional to the grain acceleration and that the magnetic field and particle velocity in a seismic shear wave are roughly proportional; Garambois and Dietrich (2002), by extending the GRMT method to deal with coupled seismic and electromagnetic wave propagation in fluid-saturated stratified porous media, thoroughly analysed seismoelectric conversions. The authors concluded that the information contained in signals arising in conversions at interfaces generated by contrasts in porosity, permeability, fluid salinity, and fluid viscosity, should be useful in hydrocarbon exploration and environmental studies. Similarly, Pride and Garambois (2005) produced numerical evidence that compressional or shear waves traversing an interface in which any of the transport properties or elastic moduli change, give rise to electromagnetic disturbances that can be measured at the surface. In particular, they observed that the amplitude of the converted electric field at the interface can be drastically increased if there is a thin layer of third material present at the interface (Fig. 11), and suggested that this feature could be exploited in hydrological applications.

5.2 2-D modelling in vertically and laterally heterogeneous media

Several works implementing different numerical methods already exist to solve the set of equations modeling both mentioned processes. Among others, Han and Wang (2001) introduced a fast finite-element algorithm to model – in the time domain – diffusive electric fields induced by SH waves, producing responses of 2-D reservoirs. The authors were able to confirm the existence of the conversions at interfaces predicted

2590

by the theory, and concluded, as other authors, that the detection of the induced EM fields should be performed with antennas positioned close to targets of interest, preferably in boreholes. This FE code, however, predicts the existence of a strong coseismic electric field in the SH analyzed mode, which collides with widely accepted theoretical demonstrations denying this fact.

Haines and Pride (2006) developed a finite-difference algorithm capable to model seismoelectric conversions in two dimensional heterogeneous media; they showed that the seismoelectric interface response from a thin layer (at least as thin as one twentieth the seismic wavelength) is considerably stronger than the response from a single interface, and that the interface response amplitude falls off as the lateral extent of a layer decreases below the width of the first Fresnel zone. The first of these conclusions was also observed in Pride and Garambois (2005), with results obtained using the GRMT. Yeh et al. (2006) developed a transition matrix approach for an electroporoelastic medium, which is based by establishing a relation between coefficients of incident and scattered waves; however, this methodology has not been used in modeling realistic geophysical situations. In Santos (2009) and Santos et al. (2012), a collection of finite-element algorithms was presented to numerically solve both electroseismic SHTE and PSVTM modes of Pride's equations. The semi-discrete version was used to analyse seismic responses of partially saturated gas/oil reservoirs in Zyserman et al. (2010), and extended to deal with gas-hydrated subsurface regions in Zyserman et al. (2012). Here it was observed that the electromagnetic seismic-induced interface response is sensitive to the saturation of gas-hydrates, as it is shown in the SHTE mode for solid accelerations traces (Fig. 12), for a gas hydrate reservoir located below the permafrost base. In Singarimbun et al. (2009), a finite differences algorithm to calculate 2-D seismoelectric responses using the transfer function was presented, and several aquitard geometries analyzed. The proposed methodology was able to image layers from the arrival of the reflected coseismic field. However, the failure of this algorithm on simulating the interface response is a disadvantage. In Ren et al. (2010), a technique extending the Luco–Apsel–Chen (LAC) generalized reflection and transmission

2591

method was introduced to simulate coupled seismic waves and EM signals radiated by point sources in layered porous media. Later, Ren et al. (2012) adapted this technique to study coseismic EM fields induced by seismic waves originated by a finite faulting in porous media. They showed that the point source approximation is not accurate in the presented configuration, and also concluded that the porosity, the solid and fluid densities and the frame shear modulus have effects on the velocity and wave amplitude of both seismic waves and coseismic EM fields, whereas the salinity only affects the amplitude of the latter.

Kröger et al. (2014), using a displacement-pressure formulation for the poroelastic part of Pride's equations, solved their 2-D fully coupled version implementing an implicit time stepping finite element algorithm in a commercial software. They analyzed *P*–*TM* conversions that occur within and at confined units. In Fig. 13 the *z* component of the induced electric field for units with different sizes presenting electric conductivity contrast with the host rock are shown. The authors demonstrated that the various seismoelectric fields capture both the structural and functional characteristics of the converting units such as clay lenses embedded in an aquifer or petroleum deposits in a host rock, thereby indicating the potential value of the seismoelectric method for exploring confined targets encountered in hydrogeological and/or hydrocarbon studies.

5.2.1 Borehole geometries

Several modeling works have been developed in borehole geometries. In Hu and Wang (2000) and Hu and Liu (2002), where simplified versions of Pride's equations were considered – by ignoring the influence of the converted electric field on the propagation of acoustic wave, i.e., neglecting the electroosmotic feedback –, coseismic electric fields for the compressional and Stoneley waves, as well as radiating electromagnetic fields were predicted. The authors proved that their simplifying assumption did not significantly diminish the quality of the modeled waves, compared to the solutions to Pride's fully coupled equations. This fact has been afterwards used by several authors, because it greatly facilitates the numerical analysis of the seismoelectric conversions.

2592

Markov and Verzhbitskiy (2004, 2005) used this hypothesis when developing an analytic approach to calculate the electromagnetic fields induced by an impulse acoustic source. They obtained, in the frequency range of acoustic logging, the relationship between the components of the induced electromagnetic field and the formation porosity and permeability; which they asserted could be potentially used for rock permeability estimation.

Pain et al. (2005) used a time domain mixed displacement-stress finite element method to model electric fields induced by acoustic waves in and around a borehole; for a maximum source displacement of one micrometer within the borehole, they predicted electrical potentials of tens of mV in the surrounding formation; and concluded that this size of signal would make such investigations viable in the field. However, they did not delve in the dependence of the measured signals with properties of the formation, the fluid and other conditions present in the borehole.

Zhan et al. (2006b) performed both laboratory experiments and numerical studies on seismoelectric and acoustic signals when studying how to eliminate borehole logging-while-drilling (LWD) tool modes, concluding that LWD seismoelectric signals do not contain contributions from the tool modes, and that correlating the LWD seismoelectric and acoustic signals, the tool modes can be separated from the real acoustic modes, improving the signal to noise ratio in acoustic LWD data.

Zhou et al. (2014) studied the seismoelectric field excited by an explosive point source located at the outside of a borehole; they observed that when the distance from the acoustic source to the axis of a borehole is far enough, the longitudinal and coseismic longitudinal wave packets dominate the acoustic and electric field, respectively. They asserted that the distance from the point where the maximum amplitude of the axial components of electric field is recorded, to the origin of coordinate indicates the horizontal distance from the explosive source to the axis of vertical borehole, and suggested that this knowledge could lead to apply seismoelectrics in microseismics and crosshole experiments.

2593

Zyserman et al. (2015) modeling shear wave sources in surface to borehole seismoelectric layouts, and employing two different models for the saturation dependence of the electrokinetic coefficient, studied the interface response of layers containing different saturations of CO₂. They observed that the IR are sensitive to CO₂ saturations ranging between 10 and 90 %, and that the CO₂ saturation at which the IR maxima are reached depends on the aforementioned models. Moreover, the IR are still sensitive to different CO₂ saturations for a sealed CO₂ reservoir covered by a clay layer.

5.2.2 Permeability dependence analysis

In a work combining modeling and field experiments, Mikhailov et al. (2000) measured Stoneley-wave-induced electrical fields in an uncased water well drilled in fractured granite and diorite. Using Biot-theory-based models, the authors concluded that the normalized amplitude of the Stoneley-wave-induced electrical field is proportional to the porosity, and the amplitude versus-frequency behavior of this electrical field depends on the permeability of the formation around the borehole.

Considering the same geometry, but analyzing the acoustic response to an electromagnetic source, electroacoustic logging for short, Hu et al. (2007) analytically proved in this context that the electrokinetic feedback can be neglected in Pride's equations, so that the reciprocal seismoelectric phenomenon could also be more easily handled. They distinguished four different mechanical wave groups generated through the conversion; in particular they paid attention to Stoneley waves, observing that their amplitude is permeability and porosity dependent. The authors noticed that the electroacoustic Stoneley wave amplitude dependence with porosity has different regimes depending on the permeability; namely it increases with porosity in the permeability range of sediment rocks, and decreases with porosity for high permeabilities (several Darcies or higher). Moreover, they noticed that in the last regime there is a threshold permeability beyond which the electroacoustic Stoneley wave amplitude does not change with porosity, and that its permeability sensibility is higher than what is observed in conventional acoustic logging.

2594

Guan and Hu (2008) used the mentioned simplification when proposing a finite-difference method with perfectly matched layers (PML) as boundary conditions for electroseismic logging in an homogeneous fluid-saturated porous formation. Since the frequency range in this work was assumed to be of the order of the kHz, the dynamic permeability was assumed to be frequency dependent, as derived in Johnson et al. (1987). Although they did not implemented it, they discussed how to extend the finite differences algorithm to deal with stratified media. Recently, Guan et al. (2013) proposed a permeability inversion method through the existing relation between seismoelectric logs and formation permeability. By working with Stoneley wave ratio of the converted electric field to pressure (REP) they noticed that its amplitude is sensitive to porosity, while the tangent of its phase is sensitive to permeability. They performed synthetic experiments which led them to argue that their results improved those provided by the acoustic logging inversion method.

5.2.3 Partially saturated media

An important topic when studying the conversions we are interested in, is their behaviour when produced in partially saturated media. The behaviour of the streaming potential coefficient under this condition has been analyzed in Sect. 3.2. Concerning wave propagation in partially saturated soils, Warden et al. (2013) extended Pride's theory to handle this kind of soils by making the model parameters – the streaming potential coefficient, bulk electrical conductivity, fluid viscosity, etc – saturation dependent; they compared the behaviour of these parameters using different saturation laws. Modifying the GRMT method accordingly, they used this extension to analyse the response of a capillar fringe between a totally and a partially saturated layer. The authors concluded that an IR created by a saturation contrast between sand and sandstone may be easier to detect than a seismoelectric conversion occurring at the same boundary between sand and sandstone with the two units fully saturated. Moreover, as shown in Fig. 14, they proved that the conversions depend on the type of saturation transition existing between the partially saturated and fully saturated units.

2595

Recently Bordes et al. (2015) used the same approach to derive the transfer function between the electric field and the acceleration as a function of water saturation (see Sect. 3.2).

5.3 Inversion attempts

Jardani et al. (2010) were able to model with a finite element algorithm the seismoelectric response over a stratified medium including a reservoir partially saturated with oil. Moreover, the authors generated one of the few inverse problem investigations published up to now. Their approach was a 2-D joint inversion of seismic and seismoelectric synthetic signals generated in a partially saturated oil reservoir; they concluded that, with this methodology, they could invert the permeability of the reservoir and its mechanical properties. More recently, Mahardika et al. (2012), by using a similar approach, inverted synthetic data corresponding to the occurrence of a fracking event in a two-layers system. The authors concluded that the model parameters are better determined for the joint inversion of seismic and electrical data by comparison with the inversion of the seismic time-series alone.

5.4 Full 3-D modelling

The degree of difficulty in numerically modelling both seismoelectric and electroseismic wavefields using finite sources (be they natural or man-made) and three dimensional Earth models – mainly because of the need of an extensive computing power – can be estimated by the fact that up to now there is just one published work involving such situations. In Wang et al. (2013), a time domain finite difference algorithm is presented to model 3-D seismoelectric responses to slipping faults, which deals with Biot equations using a velocity-stress FDTD algorithm and the PML technique for the truncated boundary, while the EM fields are calculated by the alternating-direction implicit method. This novel methodology was validated against analytic solutions, studying the seismoelectric fields induced by a slipping fault – modeled as a double couple – in an otherwise

2596

homogeneous semispace. In particular, the vertical component of the electric field near the surface was analyzed, due to its expected high attenuation rate in this region. Contrarywise to what they observed far from the surface, in its vicinity the numerical vertical electric field departed from the analytical results; the authors attributed this fact to a low precision approximation for the spatial variation of the pressure in their algorithm.

5.5 Data filtering techniques

5.5.1 Harmonic noise

The first step in processing the seismoelectric data is to remove the noise coming from power lines, which can be of the order of 1 mV m^{-1} . The estimate of the harmonic noise can be performed on the data recorded just before the shot, using a pre-trigger recording. The harmonic noise may be reduced by subtracting the noise recorded by a remote dipole, or using the difference between the signal recorded by dipoles symmetrically put on opposite side of the shot. The filtering of this noise can be performed by applying a single frequency adaptative noise cancellation filter. Butler et al. (1996) proposed to apply the techniques of block and sinusoidal subtraction. Note that the most efficient method which is used for most of the observations is to routinely reduce the harmonic noise using the algorithm of Butler et al. (1996, 2007); Butler and Russell (2003), applied to individual shot before the stacking. Wiener and bandpass filters can be used to reduce high-frequency noise (Thompson and Gist, 1993). Supplementary techniques as delay-line filtering in case of severe noise (Szarka, 1987), and low-pass filtering in case of strong high-frequency noise contamination can be used.

Another algorithm for suppressing power line noise is the Hum filter devised by Xia and Miler (2000). Determined using the Levenberg–Marquardt method, this filter can handle cases where power-line noise and its multiples exist simultaneously, and removes them without altering the signals spectra.

2597

5.5.2 Trigger and cables

Noise at the beginning of the records can often be recorded. It can be a problem when trying to detect shallow interfaces. This noise can be induced by the metallic plate hit with a hammer to provide the source. Using a non-metallic plate can resolve this problem (Butler, 1996). Inserting a piece of cardboard between the plate and the hammer can also eliminate this noise (Butler et al., 2007). Using an automatic triggering can also induce spikes in the signal, because there is a large difference of voltage in the cable linking the piezoelectric transducer to the trigger. Therefore a manual triggering is preferred when trying to detect shallow interfaces; otherwise we can be simply mute the first 10 ms. Possible noise from cross-talk cables must also be checked. Finally Butler et al. (2007) noted that the amplitude modulated (AM) radio interference could be reduced by reducing the contact impedance of the electrodes in the ground, using a mixture of water and soil within the holes of the electrodes.

5.5.3 Interfacial response

The interfacial response can provide information about the formations at depth while the co-seismic signal provides only informations in the vicinity of the electrodes. The challenge is therefore to isolate the interfacial response, which is often of the order of $\mu\text{V m}^{-1}$. Note that the interfacial response can be observed free of the coseismic signal when the electrodes are located below the interface of interest (Dupuis et al., 2007), by measuring the electric field within a borehole. However this situation is not commonly implemented.

Haines et al. (2007b) undertook a series of controlled seismoelectric field experiments, from which it was concluded that off-line geometry (e.g., crosswell) surveys offer a promising application of the seismoelectric method, because they allow for the separation the IR from the coseismic and source related fields; moreover, as seismic sources and electrode receivers would be positioned near to targets of interest, the use of high-frequency sources would be possible, and the recording of the signals that

2598

rapidly decay with distance because of the nature of the electric dipole field would be facilitated.

The characteristics of the IR is an opposite polarity on opposite sides of the shot, an amplitude which is maximum at offset half of the interface depth, and a quasi-simultaneous arrival on the electrodes. As the interfacial response arrives simultaneously on the electrode profile (meaning it has almost a zero slowness or infinite velocity), the co-seismic signals propagating with seismic velocities can be eliminated in theory using an F-K or tau-p filter, so that the interfacial response can be isolated. Using the F-K filtering can show good results by differentiating the IR response from the coseismic signal (Strahser et al., 2007). However such filters require a spatial sampling relatively dense, which is not often encountered. One possibility to overcome this problem has been proposed by Kepic and Rosid (2004) who combined shot records from 24 sensors from adjacent closely spaced shot positions to create a virtual 120 channel record or “super gathers”.

Haines et al. (2007a) proposed a workflow to deal with seismoelectric signals, starting with the removal of power line harmonic noise as explained above, followed by using frequency filters to minimize random and source-generated noise. The next step would be to adjust amplitude levels by using time-varying gains, followed by the separation of signal and noise, for which they proposed to use either linear Radon transform filtering or nonstationary prediction-error filters. As a final step, they suggested to perform display processing, by means of frequency filtering and gains. In the signal/noise separation stage they observed that mapping to the linear Radon domain with an inverse process incorporating a sparseness constraint worked adequately, but also that this process was ineffective if noise and signal show the same dip. They also noticed that F-K filtering not only fails to remove all source-generated noise but also perturbs signal amplitude patterns. They asserted that prediction-error filters are a better way to separate signal and noise, while also preserving amplitude information, whenever appropriate pattern models can be built for the signal and noise.

2599

More recently, Warden et al. (2012) developed a new Fast Discrete Curvelet Transform-based filtering strategy to separate IR from coseismic signals, with the goal of improving the preservation of the IR amplitudes. The authors obtained better results with their technique than when applying Radon transform or F-K filtering, confirming the critics that Haines et al. (2007a) made to the latter. They also argued that standard “dip-based” procedures taking advantage of the high ratio between EM signal propagation velocity and its seismic counterpart, can be used to identify IR. However, as previously noticed in Thompson et al. (2007), they also remarked that this choice, by altering signal amplitudes, removes the possibility of characterize reservoir geometries.

6 Field observations

Field measurements can record both the coseismic and the interfacial signals. Due to the small amplitude of the IR, and to the ambient electric noise, pre-amplifiers are needed to enhance the signal-to-noise ratio. Several geometries can be developed in the field: the source and the electrodes can be implemented on the surface or within a borehole. The field acquisition systems and geometries usually exploit the asymmetry of the IR signal to enhance the separation of the signal from the noise.

We first describe the recommendations for the sources, electrodes, and acquisition. Then we detail results showing interfacial responses, measurements performed in boreholes, electro-seismic observations, and observations for partial-saturation conditions.

Sources

Most of the academic studies are performed using a sledgehammer as the seismic source. Various hammer plates of aluminium, polycarbonate, wood, with various geometries can be used (Haines et al., 2007b). It may be better to use a non-metallic plate to avoid the electrical noise linked to the moving metallic plate into the magnetic

field when the plate is in electrical contact with the soil: this Lorentz field has been studied by Haines et al. (2007b). Then processing the data requires the stacking of about 100 records to be able to detect interfacial response, even at typical distance of 20 m (Haines, 2004). Other seismic sources as explosives (Thompson and Gist, 1993) or accelerated weight drop (Dupuis et al., 2007) are also used. The amplitude of the IR signal was shown to be proportional to the square root of the charge weight, the amplitude of the seismic first break showing the same proportionality (Martner and Sparks, 1959). A vibrator-source tested by Haines (2004) showed too much electrical noise to be used. Several records can be combined to improve the signal-to-noise ratio (Kepic and Rosid, 2004; Dupuis et al., 2007; Strahser et al., 2011). The triggering using the electric signal of the output of an accelerometer mounted on a hammer can generate electromagnetic noise. A manual triggering does not induce this noise. Data acquisition can also be triggered by the light that accompanies cap detonation, and transmitted by a fiber optic cable (Butler et al., 1996), to avoid this noise.

Recently an hydraulic vibrator has been used to increase the source strength (Dean et al., 2012; Valuri et al., 2012) on two sites: in Australia and in Abu Dhabi. The authors showed that the interfacial response due to a water table at depth of about 14 m could be detected without stacking, at offsets of up to 120 m, on the first site (Dean et al., 2012); and that the coseismic signal was clearly shown on a large scale in the arid region of the second site (Valuri et al., 2012). Moreover, when the data were stacked the interfacial response of the base of the aquifer, at a depth between 40–60 m, was shown on a profile up to 800 m (Dean et al., 2012).

Electrodes

The electrode polarization is less a problem in seismoelectric than in other geophysical methods such as Audio-Magneto-Tellurics or Self-potentials. The seismoelectric signals obtained with polarizable (stainless-steel, lead rods) or non-polarizable (Cu/CuSO₄) electrodes do not differ significantly from each other (Beamish, 1999). Electrodes are often stainless steel tubings of 30 to 50 cm length. The contact

2601

impedance between electrodes must be low, which needs the electrodes to be watered when the soil is not wet enough. Some authors suggest to water the electrodes with a mixture of clay and water. The dipole length is usually 1 to 2 m. The effect of the dipole length between 1 and 10 m has been tested: the amplitude results showed that the received voltages are independent of dipole length when the position of the inner (nearest the shot point) electrode remains at a fixed offset, the inner electrode controlling the amplitude and character of the received voltage (Beamish, 1999), as already mentioned by Martner and Sparks (1959). Data collected with and without geophones present between two electrodes are similar, so that the geophones do not affect the seismoelectric signal (Haines, 2004). When measuring the seismoelectric conversions within a borehole, Dupuis et al. (2009) used tinned copper wire wrapped around segments of PVC pipe of 10 cm long and 2.5 cm in diameter.

Acquisition

Most of the data acquisition systems are modified and unmodified multichannel seismic systems. Signal conditioning can use fixed or variable gains, and different bandwidths. The data sampling can range from 10 to 20 kHz, the resolution is 16 bit and the typical record length is 4000 points. Pre-amplifiers should be used, with high input-impedance and high common-mode rejection, so that the correct amplitude of the signal can be detected, and can be compared from one observation to another including different soil conductivities. However such pre-amplifiers are not always used, so that the amplitudes of the field observations are often not comparable. At least the impedance across a pair of electrodes should always be tested to be several orders of magnitude less than the input impedance of the acquisition system. Moreover the acquisition system can be grounded to avoid spurious instrument-related noise.

6.1 Interfacial response observations

Over the past decades seismoelectromagnetic phenomena have been observed in the field, as recalled above in the History section. Then over twenty years and recently, increasing successful field experiments have been reported.

5 Seismoelectrics have been used for mapping a shallow lithological boundary (Butler et al., 1996). These authors could map an interface between permeable organic-rich road fill and impermeable silty glacial till. Using a hammer source or detonation of blasting caps at various depths in a borehole (from the surface to 5 m depth), they could map a dipping interface between 1 and 3.5 m depth. The amplitude of the recorded signals, 10 using a sledgehammer, was in the range 0.8 to 2.4 mV for dipoles of 10 m length. When using the detonation source in the borehole, the amplitude of the recorded dipoles at the surface was 3 mV to 20 μ V for 2 m dipoles. The maximum offset was about 10 to 20 m. The water table present at 1 m below the interface or 0.35 m above the interface was not detected by a seismoelectric conversion. The authors concluded that seismo- 15 electrics may be used to map the interface of permeable layers.

Seismoelectric surveys were also performed on a subsurface site known by seismic refraction and resistivity (Mikhailov et al., 1997). The authors observed the IR at the top soil-glacial till interface at 0.75 m depth, and also the signal induced by the electric field generated by the seismic head wave traveling along this interface, which shows 20 a moveout on the recordings. They could also detect the water table at 3 m depth and the glacial till–bedrock interface at 9 m depth. After filtering the data the amplitudes of these signals are from 300 to 5 μ V from 0.6 to 6 m from the source.

Garambois and Dietrich (2001) measured the IR from a water table at about 1.5 m depth, and the electric signals associated to the Rayleigh surface waves which dominates the observations. The authors showed that the amplitude of this second signal 25 depends on the local properties of the porous medium, as explained by the derivation of the transfer function (see Sect. 3.3). The coseismic signals could therefore help to characterize the properties of the fluid of the local porous medium.

2603

Seismoelectric surveys have also been performed for the exploration of glaciers, as on glacier de Tsanfleuron (Switzerland). The interface between snow and ice at about 22 m depth, with a difference in seismic velocity from 960 to 3650 m s^{-1} , was identified by an IR detection (Kulesa et al., 2006). Moreover the ice-bed (limestone) interface at 5 about 95 m depth also induced an IR.

Strahser et al. (2007) performed seismoelectric survey in Holocene sediments from Fuhrberg forest (North Germany), by measuring radial, transverse, and vertical components of the seismoelectric field. Data were first filtered through F-K transform. Then the polarisation of the seismoelectric field was analysed. The coseismic wave is polarised perpendicularly to the front of the P wave time derivative, and the IR field is 10 polarised as the field lines of an electric dipole source. The IR from a sand/silt interface at 4 m depth could be detected. The relative amplitude between radial and vertical components of the seismoelectric field could be modeled only by taking into account the destructive interference of the IR originating at the interface at 4 m depth and at 15 another interface at 5 m depth. This thin layer would have been remained undetected with one-component measurements.

Dupuis et al. (2007) built a seismoelectric profile acquired over 300 m on sedimentary context (Fig. 15), by plotting at each shot location the stack of the traces with offsets between 14 and 40 m. A water table at depth 14 m and a shallower water-retentive 20 layer in sediments were detected. The authors observed a peak amplitude of 1 $\mu\text{V m}^{-1}$ and the IR was detected at offsets up to 40 m from the seismic source. Note that the shallow water-retentive layer was not mapped by seismic reflection or refraction. The authors concluded that the seismoelectric method can be a valuable tool for the characterization of aquifers.

25 It is possible to record the IR separately from the coseismic field by building two trenches filled with sand and apart of 2 m within a clay-rich soil, as performed by Haines et al. (2007b). These authors performed off-line geometry surveys using seismic shots on the opposite site of the receiver profile, compared to the two trenches, with an angle

2604

of 20°. The authors clearly showed the interface signals from the trenches in their correct dip geometry.

6.2 IR observations using borehole geometry

A great advantage of a vertical seismoelectric profile is the possibility to perform the measurements below the studied interface, so closer to the interface and allowing for the separation of the IR from the coseismic signal. Electrodes can be deployed within a water-filled borehole. In this case the borehole should have a slotted PVC casing to allow the electric contact between the electrodes and the formation.

Decades ago Martner and Sparks (1959) performed explosive detonation in borehole, at several depths up to 60 m and measured an IR, either by electrodes on the surface or within another hole. They showed that the IR was generated by the base of a weathered layer, at about 3 m, characterized by a change in seismic velocity.

Later on Butler et al. (1996) could map a shallow lithological boundary using blasting of fuse caps within a borehole as the seismic source. The interface between an upper till layer over a glacial till at about 2 m depth was clearly shown by the seismoelectric signals measured at the surface. These authors showed that when the source is below the interface the seismoelectric signals have higher amplitude and higher frequency responses than when the source is located above the interface. The authors concluded that it was due to a better seismic coupling in the dense glacial till than in the upper layer. Russell et al. (1997) noted that the IR conversion could be detected up to offsets of 16 m, and that the top of the bedrock also induced an IR conversion.

Electrokinetic response in borehole can also be used to detect fractures, as proposed by Hunt and Worthington (2000). These authors used a mechanical source consisting of a steel tube through which runs a steel shaft attached to a cylindrical nylon block, which was pulled up by a rope up to the surface. This system has the advantage to avoid the electrical noise that may arise from electromechanical mechanism. The induced pressure pulse gives rise to an electrokinetic signal measured by steel mesh electrodes within the borehole. The authors measured electrokinetic signals up

2605

to 1500 mVMPa⁻¹ and showed strong correlations between the electrical signals and the location of opened fractures in the range 1 mm–5 cm.

More recently Dupuis et al. (2009) could detect a partially cemented layer of 2 m height within unconsolidated sediments at about 13 m depth, by a vertical seismoelectric profiling survey, using a sledgehammer seismic source on surface and six electrical dipoles within the borehole. The advantage of this configuration is that the noise level is as low as 0.1 to 5 µV m⁻¹. Over the two locations investigated, only one showed very clear IR signal, observed over more than 14 m depth. This signal was interpreted to be due to a sharp increase in fluid conductivity and a strong impedance contrast from the water table and a coincident partially cemented layer.

6.3 Electroseismic observations

The electroseismic surveys use an injection of current into the earth in the seismic frequency band. The spacing of the electrodes is similar to the depth of investigation. The converted seismic wave is then recorded by geophones on the surface or in a borehole. The commonly understood conversions vary linearly with the input current. Electroseismic observations are less common than seismoelectric ones, maybe because of the difficulty of injecting a large enough current (which can range from one hundred to one thousand A) with appropriate characteristics. The challenge in building the electromagnetic source is that the current level can be thousands A and the switching time resolution is tens to hundreds of µs. The near-surface noise coherent with the source could also be a limitation.

Decades ago, Thompson and Gist (1993) observed conversions from electromagnetic to seismic energy at the siliciclastics Friendswood test site (Texas), with the presence of a sequence of high permeability water sands and low permeability shales over 300 m depth. Electric currents of 150 A were injected through electrodes of aluminium foil of several meters buried 0.5 m below the surface and separated by 300 m. Pulse frequency signals were applied with a 20 kW audio power amplifier. The hydrophones

were shielded to reduce the electromagnetic pick up. Seismic measurements were performed within a borehole located between the two source electrodes. Unfortunately the authors could not have enough data to process an imaging of the interfaces. They showed through modelling that electroseismics are more sensitive to low permeability formations whereas seismoelectrics are most sensitive to high permeability formations.

Over the last two decades some observations showed that the electroseismic conversions could yield conversions of higher energy efficiency. First successful demonstration that electroseismic conversions can distinguish between aquifers and gas sands and can be used at depths up to 1000 m using geophones placed on the surface of the earth were provided by (Thompson et al., 2007; Hornbostel and Thompson, 2007). Source waveforms have been developed through coded waveforms, both with a linear and nonlinear sequence of 60 Hz cycles. These developments were performed to consider the case in which the linear limit is exceeded, in which the seismic response is proportional to the square of the input current (Hornbostel and Thompson, 2005). Some power waveform synthesizers were developed, each handles 350 kW and weighs 300 kg. Digital accelerometers were used to achieve the low electromagnetic pickup required to detect the small IR signals, and were deployed on the surface or in borehole (Thompson et al., 2007; Hornbostel and Thompson, 2007).

Observations were performed on the Webster field (Gulf coast, Texas) whose gas sands showed porosities of up to 34 % (Thompson et al., 2005). Electroseismic IR were detected at least for three sand intervals up to 150 m depth. The IR signal was strengthened when the channel was filled with shale. The authors showed through modelling that, because the gas sands are high-resistive, electric currents can steer around so that the IR is weak for a thick layer and strong for a thin layer. Moreover the observations showed that the high-amplitude electroseismic conversions were associated with gas sands, and showed the power of resolving fine structure of 5 m difference between shale and gas sand (Thompson et al., 2007). This experiment succeeded to detect gas sands up to 500 m deep with good signal-to-noise ratio.

2607

Another survey was performed in the Turin field (Alberta), having porosities as high as 28 % and permeabilities up to 4 Darcies (Thompson et al., 2005). Both surface and downhole (hydrophones) measurements were performed. It was observed at one location an IR related to the lower limit of a shallow thick (35 m) highly-resistive gas cap at 1000 m depth.

A third field was investigated by the same authors, the Bronte field (Texas) which is a deeper carbonate oil reservoir with porosities ranging from 6–12 % and permeabilities 7–200 mD. The reservoir was not detected by the linear electroseismic conversion. Nonlinear response was observed showing coherent amplitudes in a portion of the survey area with hydrocarbons where production occurs, which was not well understood (Hornbostel and Thompson, 2007). Further analyses showed that the electroseismic conversions included source-generated noise (Thompson et al., 2007). The authors processed the signal at double the source frequency to reject the fundamental frequencies of the source waveform. The high-amplitude ES conversion at 1500 m depth was shown to match well the seismic studies. The authors concluded that it is not obvious that the electrokinetic conversion process can account for these second-order effects.

6.4 Partially saturated observations

Strahser et al. (2011) observed seismo-electric conversions in the field, as a function of water-saturation, and proposed a transfer function between the electric field and the acceleration as a function of the water-saturation. The authors proposed that in the low frequency domain, taking into account the water saturation, the seismoelectric field and the seismic field are related as:

$$\mathbf{E} \simeq \frac{\epsilon \zeta}{\eta \sigma_f} S_e^{(0.42 \pm 0.25)\eta} d_f \ddot{\mathbf{u}}. \quad (34)$$

The observations could not be performed in a large range of water-content, leading to relatively scattering data. This approach has to be compared with recent results from Bordes et al. (2015) in Sect. 7.1.

7 Laboratory observations

- 5 Due to the low signal-to-noise ratio of the seismo-electromagnetic conversions, laboratory measurements are difficult. It is first necessary to exclude the seismoelectric resonance effects caused by mechanical vibrations of the sample itself. It is therefore essential to have a rigid framework. Moreover the electric and magnetic recorders must be mechanically decoupled from the sample setup, so that they can not vibrate.
- 10 Some experimental setups include an absorber of acoustic signals which strongly reduces the effect of reflected waves on the results of measurements in the harmonic regime (Migunov and Kokorev, 1977). The electromagnetic noise must be suppressed by shielding the setup and the wires. Some experiments are carried out in a specially shielded room, or copper mesh Faraday cage can be used to isolate the experimental
- 15 device from electrical interference and to provide a universal ground. When performing magnetic measurements it is necessary to use non-metallic materials, because of their possible even small displacements within the ambient magnetic field. Measurements performed on dry samples showed that both the electric field and the magnetic field are within the noise level (Zhu et al., 2000; Bordes et al., 2008).

20 Sources

- Due to the scale of the samples used in laboratory, the seismic source is usually higher frequency, in the range of 10–500 kHz, than the frequencies involved in field observations. In most of the studies piezoelectric transducers are used to generate *P* waves and *S* waves. Although the center frequencies of the transducers are several hundreds of kHz, the center of frequencies of the propagating wave can be about 20 kHz
- 25

2609

- (Zhu et al., 2000), because of attenuation. The acoustic transducers are driven by an electric pulse, whose width is adjustable usually to the half period of the recorded acoustic wave and can be in the range 10 to 100 μ s. This pulse can be a single pulse, a continuous sine wave or a multi-cycle sine bursts. In case of a cylindrical sample
- 5 whose length is very large compared to the diameter the main modes excited can be the extensional and flexural ones.

Electrodes

- Different kinds of electrodes can be used. Electrodes can be made of conducting glue of 0.2 cm of diameter (Zhu et al., 2000), of platinum discs, of impolarisable silver/silver
- 10 chloride rod, or mesh.

Equilibrium time

- The equilibrium between the sample and the water must be attained to be able to reach the steady state. This equilibrium should be checked by measuring the pH and the electrical conductivity of the fluid while water is circulating within the sample (Guichet et al.,
- 15 2006; Schoemaker et al., 2008; Allègre et al., 2010), and performing the electric measurements once the pH and conductivity are constant. If the equilibrium is not attained the electric measurement can be not constant. Moreover measurements performed at different salinities could be difficult to compare (Schakel et al., 2011, 2012).

7.1 Effect of physical parameters on seismo-electric conversion

- 20 In the 1970s, laboratory experiments were performed to better understand the effect of salinity, of moisture, of porosity, and of frequency on the coseismic signal (Gaskarov and Parkhomenko, 1974; Migunov and Kokorev, 1977)

- Most of the time, only the longitudinal seismoelectric conversion is measured: when the electric field is parallel to the propagation of the elastic wave. Parkhomenko and
- 25 Topchyan (1995) measured also the transverse seismo-electric effect by measuring

2610

the electric field by two electrodes moving along the surface of the sample perpendicular to the wave propagation induced by a piezoelectric transducer. It was shown that the projection of the electric intensity vector on the direction perpendicular to the direction of elastic wave propagation is about one order smaller than the projection on the direction of the wave propagation.

The effect of the frequency of the seismic source was studied on limestone samples with about 8–10 % water-content, maintaining a constant acoustic intensity. Measurements showed that the magnitude of the seismoelectric signal increases with frequency in the range 5–25 kHz. On the other hand recent results showed that the amplitude of the seismoelectric coefficient decreases when the frequency increases in the range 5–200 Hz on glued glass-tubes samples, and that the phase values also decrease with increasing frequency (Schoemaker et al., 2008). These observations are in accordance with the theory of Pride. Moreover it was also shown that the amplitude of the seismoelectric coefficient decreases when the frequency increases in the range 15–120 kHz on a saturated Berea sandstone with NaCl solutions with conductivities between 0.012 to 0.32 S m⁻¹ (Zhu and Toksöz, 2013), which is in accordance with the theory for saturated conditions (Eq. 8). For a conductivity of 0.012 S m⁻¹ the seismoelectric coefficient is decreased from 0.25 to 0.15 μV for an increasing frequency from 15 to 120 kHz respectively (Zhu and Toksöz, 2013). The different results of these studies show that the effect of water-content may be complex.

Three values of porosity were tested by Migunov and Kokorev (1977): 4, 10 and 12 % at water-content 8–10 % and the slope of the electric signal-frequency curve increases with porosity. The effect of porosity has been studied on the same samples of limestones, and the magnitude of the seismo-electric signal increases with increasing porosity in the range 4–12 % (Migunov and Kokorev, 1977). But another study showed a decrease of the seismoelectric effect with increasing porosity on limestones and sandstones (Ageeva et al., 1999).

The effect of salinity was studied on samples of limestone, sandstone, aleurolites and marl at frequencies of 25 kHz or 60 kHz. It was observed a decrease in the seismo-

2611

electric effect with increasing concentration C of the NaCl solution saturating the rocks (between 0 and 150 g L⁻¹). This dependency is exponential, the strongest changes being between 0 and 40 g L⁻¹. The authors proposed, based on their observations, that the electric signal depends on the concentration C [g L⁻¹] as $\log V = a \log C + b$ (Gaskarov and Parkhomenko, 1974). This decrease in the seismo-electric signal with increasing salinity was explained according to the Helmholtz–Smoluchowski relation (Eq. 22), because of: (1) a decrease in zeta potential due to a decrease in the thickness of the diffuse layer, (2) an increase in the fluid conductivity, (3) an increase in the fluid viscosity. We note that this interpretation is in coherence with the transfer function (Eq. 16). More recently Zhu et al. (2000) showed a decrease in the seismoelectric signal with decreasing sample resistivity in the range 50 to 1000 Ω m on Berea sandstone and Coconino sandstone at frequency 20 kHz. The electric signal was measured at 90 and 50 μV for Berea and Coconino respectively for a sample resistivity of 400 Ω m. A decrease of the seismoelectric effect is also observed with increasing salinity, at full saturation on limestones and sandstones (Ageeva et al., 1999), and at water contents of 8 or 24 % on sand (Parkhomenko and Gaskarov, 1971).

The effect of moisture was studied on the samples of limestone, sandstone, aleurolites and marl. The seismoelectric potential increases with increasing moisture from 1 to 17 %. A slight decrease is observed in some samples at moisture in excess of 15 %. The inflection of this curve is shifted toward higher moisture values in proportion to the increase in the concentration of the solution (Gaskarov and Parkhomenko, 1974). Other studies showed a sharp increase at low water content, and can then be constant at increasing water content on dolomite, marl and sandstones, or can decrease on tegillate loam, morainic loam, and limestones for a frequency of the seismic source around 25 kHz (Parkhomenko and Tsze-San, 1964; Parkhomenko and Gaskarov, 1971; Ageeva et al., 1999). However, at low frequencies (400 Hz compared to 25 kHz) no decrease of the seismoelectric effect is observed with increasing water saturation. Only Ageeva et al. (1999) performed measurements at low frequencies (400 Hz), but they normalized the seismoelectric signal to the response of the source

2612

of the elastic waves (the test transducer, in V), so that the coseismic transfer function (Eq. 16) cannot be deduced.

Recently the effect of water saturation on coseismic seismoelectric signals was studied on sand (Bordes et al., 2015), using as seismic source a steel ball hitting a granite cylinder in contact with the sand (Sénéchal et al., 2010). The main frequency content of this source was about 1.5 kHz and induces direct *P* wave (Barrière et al., 2012). The electric signal was recorded by electrodes dipoles (10 cm apart) along the *P* wave propagation, using pre-amplifiers and dynamic acquisition modules PXI-4498 (National Instruments) at a 200 kHz sampling rate. Experiments were performed during imbibition and drainage for several cycles, and the water-content was measured by capacitance probes. The authors estimated the transfer function of the electric field (electric field over acceleration) by picking the arrival in time domain, and by a spectral analysis using continuous wavelet transform. Both methods show that these ratios are of the order of $2\text{--}7 \times 10^{-4} \text{ V m}^{-2} \text{ s}^{-2}$ (depending on the offset to the source) and are rather constant in the water saturation range 0.2–0.9 for imbibition and drainages experiments. None of the tested models for the water-saturation dependence of the SPC could model correctly a constant transfer function in this range of saturation.

7.2 Interfacial response detection

With further developments in the sensitivity of the data acquisition systems, it became possible to detect both the coseismic seismo-electric signal and the interfacial response.

Chen and Mu (2005) developed an experimental setup composed of a plexiglass box with sand, a piezoelectric transducer excited by an electric square pulse (760 V amplitude and 10 μs width) emitting *P* wave with a main frequency of 463 kHz, and platinum disc electrodes (Fig. 16). The electrodes are connected to a preamplifier and the electric field is recorded by an electromagnetic instrument with a sampling rate 0.1 μs . The authors showed that the amplitude of the coseismic conversion within the sand decreases with the increase of the distance between the source and the elec-

2613

trode (Fig. 17) and is in the range 10–180 μV . According to Eq. (16) the seismoelectric signal becomes weaker when the concentration of the electrolyte is increased, as observed by the authors. Moreover the seismoelectric signal is proportional to the grain acceleration, so that the seismoelectric signal is decreased with the increase of the source-receiver offset, the emitting acoustic energy being lower. Chen and Mu (2005) observed both the first kind of seismo-electric conversion in sand, and the interfacial seismoelectric conversion between contrast in NaCl solution/NaCl saturated quartz and water-saturated sand/NaCl saturated sand. They observed an amplitude of the interfacial response in the range 5–10 μV .

Another study was performed, by Block and Harris (2006), on sand to detect the interfacial response between water and saturated sand. The experimental setup developed is a cylindrical PVC tube (2 m height), with nine Ag/AgCl electrodes. The source is a 100 kHz submersible acoustic transducer driven by a sine wave (Fig. 18). The electric signals are amplified 60 dB, averaged 1000 times, and filtered with a band-pass between 2 and 500 kHz to remove unwanted noise. The authors observed the first kind of seismo-electric conversion which is the transmitted acoustic wave corresponding to the Biot fast wave (Fig. 19), and also the interfacial response (IR). This electric signal is generated at the fluid–sand interface, propagates at the velocity of the electromagnetic wave in the fluid and sediment, and is recorded almost simultaneously at each one of the electrodes along the vertical array (Fig. 19). The amplitude of this IR is about 200 μV within the water and about 800 μV within the sediments for a water conductivity of $5.2 \times 10^{-3} \text{ S m}^{-1}$, and about 20 μV within the water and 500 μV within the sand for a water conductivity 7.6×10^{-3} . The authors deduced the peak of the efficiencies (in nV Pa^{-1}) of the fast wave potentials as a function of the bulk conductivity (Fig. 20) and the IR responses of about 100 μV correspond to efficiencies greater than 30 nV Pa^{-1} .

Liu et al. (2008) detected a seismoelectric conversion at a frozen–unfrozen interface. The authors developed an experimental setup with an upper frozen sand layer over an unfrozen sand layer saturated with water. The acoustic sources are 48 kHz *P* wave source transducers driven by a square electric pulse with a width of 100 μs .

They are located at the surface of the upper layer and can be used as near and far sources. The electric field is measured by six electrodes located at the bottom of the frozen layer. The coseismic conversion linked to the electric field moving along with the acoustic wave propagation in the frozen part was detected, and its amplitude decreases with the increasing temperature of the frozen sand layer from -8 to -4°C . The maximum amplitude is of the order of $100\text{ }\mu\text{V}$. The authors suggested that this localized signal may have an origin in the electromagnetic induction rather than a local streaming potential because the frozen part is a non-conductive medium. The interfacial response was also detected, but only after 8 h of the interface being formed. The authors concluded that the formation of the electric double layer at the interface requires typically a duration of several hours.

Schakel et al. (2011) detected an interfacial response between water and a glass porous sample inside a water tank. They measured the waveform and the amplitude of the IR parallel and perpendicular to the interface. In this geometry the electric field is created only by the conversion from the interface, so that there is no interference with the body wave coseismic fields. They showed a decrease of the signal with increasing distance to the interface, and a decrease of the signal on both side of the excitation point along the interface, resembling to the pressure pattern. These waveform and spatial amplitude pattern could be well reproduced by a source pressure modelling based on the Sommerfeld approach and the theory of Pride, taking into account only the reflected electric potential wave, whereas the approximation of the electric dipole overestimated the amplitude decays.

Recently, using the same experimental setup, an interface between an oil-saturated and a water-saturated porous glass filter samples was detected (Smeulders et al., 2014). As the oil-water front moved, this initial interface vanished and the corresponding IR also vanished. Therefore this experiment showed that a purely mechanical contrast at the interface without electrical contrast in these conditions could not induce a detectable IR. Moreover the authors could detect an IR between a water-saturated Fontainebleau sandstone and a water or oil layer. The amplitude of the interface

2615

rock/water was measured to be about $50\text{--}75\text{ }\mu\text{V}$, and the one of the interface rock/oil was about $10\text{ }\mu\text{V}$. Although the oil conductivity is lower than the water conductivity, the electric contrast between the water-saturated sandstone and oil may be lower than the one between the water-saturated and the water, leading to a decrease of the amplitude of the IR.

7.3 Seismo-magnetic detection

To measure the magnetic field, induction detectors of the selenoidal and toroidal types can be used, and make it possible to measure the axial and transverse components of the magnetic field. Migunov and Kokorev (1977) showed that the seismoelectric signals recorded by the induction detectors have the same form as the signal recorded by electrodes, but are weaker in intensity. Note that it has been already suggested to monitor the magnetic field in boreholes to detect fluid flow variations in an accretionary prism (Jouniaux et al., 1999).

Bordes et al. (2006, 2008) showed the existence of seismo-magnetic conversions, predicted by the theory since 1994. The authors developed an experimental setup with a remote-controlled seismic source, to induce seismic wave propagation in a saturated sand column (Fig. 21). This study was performed in the Low Noise Underground Laboratory (LSBB-Laboratoire Souterrain a Bas Bruit) providing low-noise environment for the electric, magnetic, and acoustic fields. The magnetic part of the seismo-electromagnetic conversions is measured besides the electric field. The seismo-electric field is shown to be coupled to the P wave propagation and extension waves, propagating at a velocity of 1300 m s^{-1} . The seismo-magnetic field is shown to be coupled to the transverse S wave, propagating at a velocity of 800 m s^{-1} . The observed amplitudes are $10\text{ }\mu\text{V m}^{-1}$ (Bordes et al., 2006) and 0.035 nT for a 1 m s^{-2} seismic source acceleration (0.1 g) (Fig. 22). Therefore these observations confirm the theory from Pride (1994) who demonstrates that the electric field is coupled to the compressional waves and that the magnetic field is coupled to the S waves.

2616

7.4 Crosshole measurements and fracture detection

The seismo-electric conversion was also observed in model wells (Zhu et al., 1999; Zhu and Toksöz, 2003) and it was experimentally shown that seismo-electric logging could be a new bore-hole logging technique. Experimental observations using a piezoelectric source within the borehole showed coseismic signals detected by an electrode in the borehole's center or within the borehole wall (Zhu et al., 1999); it was shown that the apparent velocities of the seismoelectric signal are the same as those of the seismic waves: the Stoneley wave and the low-frequency component of the P wave. It was also shown that these seismoelectric signals were not detected or were of very low amplitude in material of low porosity and low permeability such as lucite and slate (Zhu et al., 1999).

On the other hand, Zhang et al. (2005) measured a seismo-electric conversion induced by pseudo-Rayleigh waves, in a large borehole experiment of 2 m in length, 0.5 m in diameter and 1.12 m in borehole diameter. This conclusion was deduced because of two dominant frequency crests observed in the seismo-electric signal. Moreover, contrary to the theory and modelling, only the interfacial response, linked to the borehole wall, was detected. The interfacial response was detected at 500 μV using distilled water, and at about 150–200 μV using a water of 1 S m^{-1} .

Zhu and Toksöz (2003) investigated the relationship between the interfacial signal induced at the fracture and the fracture aperture. They performed laboratory experiments in cross-borehole models using one sample of Lucite and one sample of sandstone separated by a vertical fracture. Both samples are saturated with water and the fracture is filled with water. A P wave, whose energy focuses in the horizontal direction, perpendicular to the well, is applied on the side of the Lucite block. It is shown that the amplitude of the interfacial response at the fracture is increased from 50 to 200 μV for a fracture aperture from 0.5 to 9 mm respectively, using tap water of 0.1 S m^{-1} of conductivity. And it is also shown that the seismoelectric interfacial response is induced at the sandstone side of the fracture and is generated mainly by a Stoneley wave ex-

2617

cited in the fracture. Zhu and Toksöz (2003) also investigated the effect of a dipping fracture between the boreholes (Fig. 23), and showed that the fracture position can be determined from the seismoelectric interfacial response induced at the fracture. The electric signal is measured at a fixed position when the source moves in the first block with 1 cm of increment. The results are shown in Fig. 24: a seismoelectric signal is observed with a velocity of 2600 m s^{-1} , which is the P waves velocity of Lucite. This is the interfacial response at the fracture at the sandstone side. The distance from the borehole within the Lucite to the fracture side (at position 1) is calculated from the first arrival time $25.5 \mu\text{s}$ (in trace 1), knowing the velocity in Lucite and in water (1500 m s^{-1}) and is deduced to be 4.9 cm compared to the real distance of 5 cm. The inclined angle of the fracture can also be deduced, from the time difference between the seismoelectric response of traces 1 and 8 and the vertical distance of position 1 and 8, and is deduced to be 69.2° , compared to the real inclination of 70° .

Experimental borehole investigations have also shown the utility of the seismoelectric signal to eliminate the Logging While Drilling (LWD) tool mode in order to access to the formation acoustic modes (Zhan et al., 2006b). Indeed the tool waves mode present in the LWD acoustic signal are not present in the seismoelectric signal excited by the LWD acoustic waves, because the drill string is grounded during the LWD process. Therefore the acoustic modes can be filtered by correlation between the acoustic signal and the seismoelectric signal (Zhan et al., 2006a).

7.5 Permeability deduction

A first attempt to deduce permeability from transient streaming potential measurements was proposed by Chandler (1981) in the quasi-static limit. Streaming potential and fluid pressure have identical temporal behaviour in low-frequency domain. Chandler (1981) showed that the time characteristic of the transient streaming potential could be used to deduce the diffusivity, and then the permeability.

A reliable permeability log within an experimental borehole has been deduced from electrokinetic measurements, using an acoustic source (Fig. 25). It has been shown

2618

that the normalized coefficient defined by the electric field divided by the pressure [$\text{V Pa}^{-1} \text{m}^{-1}$] depends on the permeability, through a finite element model and laboratory experiments (Singer et al., 2005). A short steel tube near the top of the borehole and hit on top with a hammer was used as the source. The main wave propagation is a Stoneley wave which induces the electric field. The logging tool is moved step-by-step within the borehole (Fig. 25). The investigated depth of such a permeability is of the order of centimeters. The normalized coefficient is coherent with the electrokinetic coupling \mathcal{L}_{ek} (Eq. 23) per unit of conductance [S]. Therefore it should increase with increasing permeability. At low permeability the fluid is not easily displaced and the oscillating source induces a larger solid displacement. However the relative movement between the fluid and the solid is limited, leading to a decrease of the electric field even if pressure increases, so that this normalized coefficient is decreased. The measured amplitude of the normalized coefficient on sandstones is in the range 1.6×10^{-7} to $2.5 \times 10^{-6} [\text{V Pa}^{-1} \text{m}^{-1}]$ increasing with increasing permeabilities from 6.2×10^{-15} to $2.2 \times 10^{-12} \text{m}^2$. This model showed that the normalized coefficient could detect a 0.5 m-thick bed of permeability 10^{-13}m^2 within a formation of permeability 10^{-15}m^2 .

On the other hand Guan et al. (2013) modeled the coseismic conversion of Stoneley waves within a borehole and showed that the ratio of the converted electric field to the pressure is sensitive to the porosity rather than to the permeability. This ratio is increased by a factor two for increasing porosity from 10 to 30 %. The Stoneley wave being sensitive to the permeability, Guan et al. (2013) further investigated the phase of the ratio of the converted electric field to the pressure, and showed that the tangent of this phase is sensitive to the permeability. They showed that the phase of the electric field always lags behind that of pressure in the frequency range up to 5 kHz and there exists a frequency about 1 kHz for which the tangent of this phase is minimum. At this frequency the tangent can be increased in absolute value by a factor when permeability increased from 500 mD to 50 mD, leading to a possible permeability inversion method. Such a permeability inversion should be tested from borehole seismoelectric signals observed in the field on in laboratory.

2619

7.6 Electro-seismic detection

The electroseismic conversion is the reciprocal of the seismoelectric conversion. It consists in applying an electric current and in measuring the induced seismic wave. It is comparable to the electro-osmosis in the frequency domain. Few laboratory studies tried to detect the electroseismic conversion.

Electroseismic “coseismic” conversions were observed in experimental saturated borehole with a Lucite block (of porosity zero) and a glued-sand (Zhu et al., 1999). The electric current was injected either within the borehole or in the borehole wall, and the P waves receiver was located within the borehole. It was shown that the induced acoustic field was a Stoneley wave.

Zhu et al. (2008) pointed out that there exists an acoustic field near the electrodes of injection, which is not an electroseismic conversion, but linked to the thermo-dilation of the water molecules when the current is injected. These authors could observe an electroseismic conversion at an interface between an epoxy-glued sand saturated with tap water over a Lucite block. The electrodes were buried in the sand and the acoustic receiver was at the bottom of the Lucite block. An electric square pulse of 500 V amplitude and 6 μs width was applied. In case of a sample immersed in a water tank, with the injection electrodes within the water, the authors suggested to better use a single sine burst wave as an electric source than a continuous sine wave, with a center frequency of 100 kHz.

8 Conclusions and perspectives

Since its foundations in the late first half of the last century, seismoelectromagnetics has experienced an important development, contributions to its deeper understanding coming from field and laboratory experiments, theoretical developments and numerical modeling. Nowadays we understand the genesis of the electrokinetic coupling and the influence of the fluids and solid matrix properties on its behaviour; the characteristics of

the electromagnetic and mechanical signals involved, their detection and processing, although the limitation of this method still remains the small level of the signals. Indeed a lot of field studies could detect shallow interface responses, whereas few studies could detect deep interfacial responses. Field observations showed the advantages of performing 3-components measurements of the seismoelectric field, and vertical seismoelectric profiles, to better detect small interfacial responses.

Recent laboratory experiments evidenced the existence of the interfacial response, at interfaces such as water/saturated porous medium; porous media saturated with different fluids (different salinities, oil); or frozen/unfrozen sand. Moreover the theoretical prediction of the seismomagnetic conversion coupled to the transverse S wave was also experimentally verified.

The results we resumed in this review show that this research area is a strong and healthy one, and that there is a number of open questions still to be addressed, for example the electrokinetic coupling under partial saturation conditions involving wetting and non-wetting fluids, the interface response created by shear waves, the detection of seismo-magnetic conversions in the field, crosshole investigations and optimized configuration, strong sources without electromagnetic noise, or enhancement of the electric signals by new electrode configurations. Moreover further numerical developments are needed for 2-D and 3-D full-waveform modelling for heterogeneous media, as for cylindrical configurations, and to move towards the inversion.

Societal questions involving a better characterisation of the fluids, and a better knowledge of the subsurface in terms of porosity, permeability, fractures, such as applications on the environment and energy domains, should gain answers from future research on this method.

Acknowledgements. We thank CNRS, CONICET, University of Strasbourg and University of La Plata.

2621

References

- Adamson, A. W.: Physical Chemistry of Surfaces, John Wiley and sons, New York, 1976. 2578
- Ageeva, O. A., Svetov, B. S., Sherman, G. K., and Shipulin, V.: E-effect in rocks, *Russ. Geol. Geophys.*, 64, 1349–1356, 1999. 2611, 2612
- Ahmad, M.: A laboratory study of streaming potentials, *Geophys. Prospect.*, 12, 49–64, 1964. 2646
- Alkafef, S. and Alajmi, A.: Streaming potentials and conductivities of reservoir rock cores in aqueous and non-aqueous liquids, *Colloid. Surface. A*, 289, 141–148, doi:10.1016/j.colsurfa.2006.04.023, 2006. 2582
- Allègre, V., Jouniaux, L., Lehmann, F., and Sailhac, P.: Streaming potential dependence on water-content in Fontainebleau sand, *Geophys. J. Int.*, 182, 1248–1266, doi:10.1111/j.1365-246X.2010.04716.x, 2010. 2580, 2586, 2610, 2646
- Allègre, V., Jouniaux, L., Lehmann, F., and Sailhac, P.: Reply to the comment by A. Revil and N. Linde on: “Streaming potential dependence on water-content in Fontainebleau sand”, edited by: Allègre, V., Jouniaux, L., Lehmann, F., and Sailhac, P., *Geophys. J. Int.*, 186, 115–117, 2011. 2587
- Allègre, V., Lehmann, F., Ackerer, P., Jouniaux, L., and Sailhac, P.: Modelling the streaming potential dependence on water content during drainage: 1. A 1D modelling of SP using finite element method, *Geophys. J. Int.*, 189, 285–295, doi:10.1111/j.1365-246X.2012.05371.x, 2012. 2586, 2637
- Allègre, V., Jouniaux, L., Lehmann, F., Sailhac, P., and Toussaint, R.: Influence of water pressure dynamics and fluid flow on the streaming-potential response for unsaturated conditions, *Geophys. Prospect.*, 63, 694–712, doi:10.1111/1365-2478.12206, 2015. 2587
- Archie, G. E.: The electrical resistivity log as an aid in determining some reservoir characteristics, *Trans. AIME*, 146, 54–62, 1942. 2581, 2586
- Auriault, J. and Strzelecki, T.: On the electro-osmotic flow in saturated porous media, *Int. J. Eng. Sci.*, 19, 915–928, 1981. 2569
- Barrière, J., Bordes, C., Brito, D., Sénéchal, P., and Perroud, H.: Laboratory monitoring of P waves in partially saturated sand, *Geophys. J. Int.*, 191, 1152–1170, 2012. 2613
- Beamish, D.: Characteristics of near surface electrokinetic coupling, *Geophys. J. Int.*, 137, 231–242, 1999. 2573, 2601, 2602, 2643

2622

- Beamish, D. and Peart, R. J.: Electrokinetic geophysics – a review, *Terra Nova*, 10, 48–55, 1998. 2566
- Beddiar, K., Berthaud, Y., and Dupas, A.: Experimental verification of the Onsager's reciprocal relations for electro-osmosis and electro-filtration phenomena on a saturated clay, *CR Mécanique*, 330, 893–898, 2002. 2569
- 5 Biot, M. A.: Theory of propagation of elastic waves in a fluid-saturated porous solid: I. Low frequency range, *J. Acoust. Soc. Am.*, 28, 168–178, 1956a. 2566
- Biot, M. A.: Theory of propagation of elastic waves in a fluid-saturated porous solid: II. High frequency range, *J. Acoust. Soc. Am.*, 28, 178–191, 1956b. 2566
- 10 Biot, M. A.: Mechanics of deformation and acoustic propagation in porous media, *J. Appl. Phys.*, 34, 36–40, 1962. 2576
- Block, G. I. and Harris, J. G.: Conductivity dependence of seismoelectric wave phenomena in fluid-saturated sediments, *J. Geophys. Res.*, 111, B01304, doi:10.1029/2005JB003798, 2006. 2582, 2614, 2655, 2656, 2657
- 15 Bordes, C., Jouniaux, L., Dietrich, M., Pozzi, J.-P., and Garambois, S.: First laboratory measurements of seismo-magnetic conversions in fluid-filled Fontainebleau sand, *Geophys. Res. Lett.*, 33, L01302, doi:10.1029/2005GL024582, 2006. 2616
- Bordes, C., Jouniaux, L., Garambois, S., Dietrich, M., Pozzi, J.-P., and Gaffet, S.: Evidence of the theoretically predicted seismo-magnetic conversion, *Geophys. J. Int.*, 174, 489–504, 2008. 2609, 2616, 2658, 2659
- 20 Bordes, C., Sénéchal, P., Barrière, J., Brito, D., Normandin, E., and Jougnot, D.: Impact of water saturation on seismoelectric transfer functions: a laboratory study of coseismic phenomenon, *Geophys. J. Int.*, 200, 1317–1335, doi:10.1093/gji/ggu464, 2015. 2577, 2596, 2609, 2613, 2645
- 25 Briggs, D.: The determination of the zeta-potential on cellulose—a method, *J. Phys. Chem.*, 32, 641–675, 1928. 2567
- Butler, K.: Seismoelectrics effects of electrokinetic origin, PhD thesis, Univ. B. C., Vancouver, Canada, 1996. 2598
- Butler, K., Russell, R., Kepic, A., and Maxwell, M.: Measurements of the seismoelectric response from a shallow boundary, *Geophysics*, 61, 1769–1778, 1996. 2567, 2597, 2601, 2603, 2605
- 30 Butler, K., Dupuis, J., and Kepic, A.: Signal to noise improvements in seismoelectrics data acquisition, *J. Phys. Chem. C*, 111, 3753–3755, doi:10.1021/jp070060s, 2007. 2597, 2598

2623

- Butler, K. E. and Russell, R. D.: Substraction of powerline harmonics from geophysical records, *Geophysics*, 58, 898–903, 1993. 2565
- Butler, K. E. and Russell, R. D.: Cancellation of multiple harmonic noise series in geophysical records, *Geophysics*, 68, 1083–1090, 2003. 2597
- 5 Chandler, R.: Transient streaming potential measurements on fluid-saturated porous structures: an experimental verification of Biot's slow wave in the quasi-static limit, *J. Acoust. Soc. Am.*, 70, 116–121, 1981. 2571, 2618
- Chen, B. and Mu, Y.: Experimental studies of seismoelectric effects in fluid-saturated porous media, *J. Geophys. Eng.*, 2, 222–230, doi:10.1088/1742-2132/2/3/006, 2005. 2613, 2614, 2653, 2654
- 10 Cooke, C. E.: Study of electrokinetic effects using sinusoidal pressure and voltage, *J. Chem. Phys.*, 23, 2299–2303, 1955. 2571
- Davis, J. and Kent, D.: Surface complexation modeling in aqueous geochemistry, *Reviews in Mineralogy and Geochemistry*, 23, 177–260, 1990. 2579, 2580
- 15 Davis, J. A., James, R. O., and Leckie, J.: Surface ionization and complexation at the oxide/water interface, *J. Colloid Interf. Sci.*, 63, 480–499, 1978. 2578, 2579
- Dean, T., Dupuis, C., Herrmann, R., and Valuri, J.: A brute-strength approach to improving the quality of seismoelectric data, *SEG Annual meeting*, 4–9 November, Las Vegas, 1–4, doi:10.1190/segam2012-0222.1, 2012. 2601
- 20 Debye, P. and Huckel, E.: On the theory of electrolytes. I. Freezing point depression and related phenomena, *Phys. Z.*, 24, 185–206, 1923. 2578
- Dukhin, S. S. and Derjaguin, B. V.: *Surface and Colloid Science*, edited by: Matijevic, E., John Wiley and Sons, New York, 1974. 2579
- Dupuis, J. C. and Butler, K. E.: Vertical seismoelectric profiling in a borehole penetrating glaciofluvial sediments, *Geophys. Res. Lett.*, 33, L16301, doi:10.1029/2006GL026385, 2006. 2565
- 25 Dupuis, J. C., Butler, K. E., and Kepic, A. W.: Seismoelectric imaging of the vadose zone of a sand aquifer, *Geophysics*, 72, A81–A85, doi:10.1190/1.2773780, 2007. 2565, 2598, 2601, 2604, 2652
- 30 Dupuis, J. C., Butler, K. E., Kepic, A. W., and Harris, B. D.: Anatomy of a seismoelectric conversion: measurements and conceptual modeling in boreholes penetrating a sandy aquifer, *J. Geophys. Res.-Sol. Ea.*, 114, B10306, doi:10.1029/2008JB005939, 2009. 2565, 2566, 2575, 2602, 2606

2624

- Fourie, F.: Aspects of the lateral and vertical resolution of surface electroseismic data with implications for groundwater exploration in fractured Karoo rocks, *S. Afr. J. Geol.*, 109, 571–584, 2006. 2574, 2575
- Fourie, F. and Botha, J.: The failure of the sounding assumption in electroseismic investigations, in: *Proceedings of the 7th SAGA Biennial Technical Meeting and Exhibition*, 9–12 October, Drakensberg, 2001. 2565, 2574
- Fourie, F., Botha, J., Grobbelaar, R., and van Tonder, G.: Application of the electrokinetic sounding technique for geohydrological investigations in a fractured rock aquifer system, in: *Proceedings of the XXX IAH Congress on groundwater: past achievements and future challenges*, edited by: Sililo, O., Cape Town, 26 November– 1 December, A. A. Balkema, 135–140, 2000. 2566
- Frenkel, J.: On the theory of seismic and electroseismic phenomena in a moist soil, *J. Phys.*, 8, 230–241, 1944. 2566
- Frenkel, J.: On the theory of seismic and seismoelectric phenomena in a moist soil, *J. Eng. Mech.-ASCE*, 131, 879–887, 2005. 2566
- Gao, Y. and Hu, H.: Seismoelectromagnetic waves radiated by a double couple source in a saturated porous medium, *Geophys. J. Int.*, 181, 873–896, doi:10.1111/j.1365-246X.2010.04526.x, 2010. 2589
- Garambois, S. and Dietrich, M.: Seismoelectric wave conversions in porous media: field measurements and transfer function analysis, *Geophysics*, 66, 1417–1430, 2001. 2574, 2576, 2590, 2603, 2644
- Garambois, S. and Dietrich, M.: Full waveform numerical simulations of seismoelectromagnetic wave conversions in fluid-saturated stratified porous media, *J. Geophys. Res.*, 107, ESE 5–1, doi:10.1029/2001JB000316, 2002. 2590
- Gaskarov, I. and Parkhomenko, E.: The seismoelectric effect in rocks and the preconditions for its application in geological prospecting work, *Izv.-Phys. Solid. Earth.*, 1, 71–74, 1974. 2568, 2610, 2612
- Gharibi, M., Bentley, L., Muller, J., and Stewart, R.: Seismoelectric monitoring of producing oilfields: a review, *CREWES Research report*, 15, 1–13, 2003. 2566
- Glover, P., Walker, E., Ruel, J., and Tardif, E.: Frequency-dependent streaming potential of porous media – Part 2: Experimental measurement of unconsolidated materials, *Int. J. Geophys.*, 2012, 728495, doi:10.1155/2012/728495, 2012. 2571

2625

- Gouy, G.: About the electric charge on the surface of an electrolyte, *J. Phys. Radium A*, 9, 457–468, 1910. 2578
- Groves, J. and Sears, A.: Alternating streaming current measurements, *J. Colloid Interf. Sci.*, 53, 83–89, 1975. 2571
- Guan, W. and Hu, H.: Finite-difference modeling of the electroseismic logging in a fluid-saturated porous formation, *J. Comput. Phys.*, 227, 5633–5648, 2008. 2595
- Guan, W., Hu, H., and Wang, Z.: Permeability inversion from low-frequency seismoelectric logs in fluid-saturated porous formations, *Geophys. Prospect.*, 61, 120–133, doi:10.1111/j.1365-2478.2012.01053.x, 2013. 2595, 2619
- Guichet, X., Jouniaux, L., and Pozzi, J.-P.: Streaming potential of a sand column in partial saturation conditions, *J. Geophys. Res.*, 108, 2141, doi:10.1029/2001JB001517, 2003. 2577, 2582, 2585, 2637, 2645, 2646
- Guichet, X., Jouniaux, L., and Catel, N.: Modification of streaming potential by precipitation of calcite in a sand-water system: laboratory measurements in the pH range from 4 to 12, *Geophys. J. Int.*, 166, 445–460, doi:10.1111/j.1365-246X.2006.02922.x, 2006. 2579, 2580, 2610, 2646
- Haartsen, M. W. and Pride, S.: Electroseismic waves from point sources in layered media, *J. Geophys. Res.*, 102, 24745–24769, 1997. 2575, 2589
- Haartsen, M. W., Dong, W., and Toksöz, M. N.: Dynamic streaming currents from seismic point sources in homogeneous poroelastic media, *Geophys. J. Int.*, 132, 256–274, 1998. 2589
- Haines, S.: Seismoelectric imaging of shallow targets, PhD thesis, Stanford University, 2004. 2601, 2602, 2641
- Haines, S. H. and Pride, S. R.: Seismoelectric numerical modeling on a grid, *Geophysics*, 71, 57–65, 2006. 2591
- Haines, S. S., Guitton, A., and Biondi, B.: Seismoelectric data processing for surface surveys of shallow targets, *Geophysics*, 72, G1–G8, doi:10.1190/1.2424542, 2007a. 2565, 2599, 2600
- Haines, S. S., Pride, S. R., Klemperer, S. L., and Biondi, B.: Seismoelectric imaging of shallow targets, *Geophysics*, 72, G9–G20, doi:10.1190/1.2428267, 2007b. 2565, 2598, 2600, 2601, 2604
- Han, Q. and Wang, Z.: Time-domain simulation of SH-wave-induced electromagnetic field in heterogeneous porous media: A fast finite element algorithm, *Geophysics*, 66, 448–461, doi:10.1190/1.1444936, 2001. 2590

2626

- Hornbostel, S. and Thompson, A.: Waveform design for electroseismic exploration, 75th SEG Annual International Meeting, Nov6-11, Houston, Expanded Abstract, 1–4, 2005. 2607
- Hornbostel, S. and Thompson, A.: Waveform design for electroseismic exploration, *Geophysics*, 72, Q1–Q10, 2007. 2607, 2608
- 5 Hu, H. and Gao, Y.: Electromagnetic field generated by a finite fault due to electrokinetic effect, *J. Geophys. Res.*, 116, 1132–1143, 2011. 2589
- Hu, H. and Liu, J.: Simulation of the converted electric field during acoustoelectric logging, 72nd SEG Annual International Meeting, Salt Lake City, 6–11 October, Expanded Abstracts, 21, 348–351, doi:10.1029/2001JB001517, 2002. 2592
- 10 Hu, H. and Wang, K.: Simulation of an acoustically induced electromagnetic field in a borehole embedded in a porous formation, Borehole Acoustics and Logging Reservoir Delineation consortis, Annual Report, Earth Resources Laboratory Industry Consortia Annual Report 2000–13, MIT, available at: <http://hdl.handle.net/1721.1/75724> (last access: 20 August 2015), 13-1–13-20, 2000. 2592
- 15 Hu, H., Guan, W., and Harris, J.: Theoretical simulation of electroacoustic borehole logging in a fluid-saturated porous formation, *J. Acoust. Soc. Am.*, 122, 135–145, 2007. 2594
- Hunt, C. W. and Worthington, M. H.: Borehole elektrokinetic responses in fracture dominated hydraulically conductive zones, *Geophys. Res. Lett.*, 27, 1315–1318, 2000. 2566, 2605
- Hunter, R.: *Zeta Potential in Colloid Science: Principles and Applications*, Academic Press, New York, 1981. 2578
- 20 Ishido, T. and Mizutani, H.: Experimental and theoretical basis of electrokinetic phenomena in rock water systems and its applications to geophysics, *J. Geophys. Res.*, 86, 1763–1775, 1981. 2579, 2583, 2584, 2646
- Ivanov, A.: Effect of electrization of earth layers by elastic waves passing through them, *Doklady Akademii Nauk SSSR*, 24, 42–45, 1939 (in Russian). 2566
- 25 Jaafar, M. Z., Vinogradov, J., and Jackson, M. D.: Measurement of streaming potential coupling coefficient in sandstones saturated with high salinity NaCl brine, *Geophys. Res. Lett.*, 36, L21306, doi:10.1029/2009GL040549, 2009. 2579, 2646
- Jackson, M. D.: Characterization of multiphase electrokinetic coupling using a bundle of capillary tubes model, *J. Geophys. Res.*, 113, B04201, doi:10.1029/2007JB005490, 2008. 2586
- 30 Jackson, M. D.: Multiphase electrokinetic coupling: insights into the impact of fluid and charge distribution at the pore scale from a bundle of capillary tubes model, *J. Geophys. Res.*, 115, B07206, doi:10.1029/2009JB007092, 2010. 2586, 2637, 2645

2627

- Jardani, A., Revil, A., Slob, E., and Söllner, W.: Stochastic joint inversion of 2D seismic and seismoelectric signals in linear poroelastic materials: a numerical investigation, *Geophysics*, 75, N19–N31, doi:10.1190/1.3279833, 2010. 2596
- Johnson, D. L., Koplik, J., and Dashen, R.: Theory of dynamic permeability in fluid saturated porous media, *J. Fluid Mech.*, 176, 379–402, 1987. 2570, 2595
- 5 Jouniaux, L.: Electrokinetic techniques for the determination of hydraulic conductivity, in: *Hydraulic Conductivity – Issues, Determination and Applications*, edited by: Elango, L., In Tech Publisher, Rijeka, ISBN 978-953-307-288-3, 307–328, 2011. 2662
- Jouniaux, L. and Bordes, C.: Frequency-dependent streaming potentials: a review, *Int. J. Geophys.*, 2012, 648781, doi:10.1155/2012/648781, 2012. 2566, 2573, 2587, 2647
- 10 Jouniaux, L. and Ishido, T.: Electrokinetics in earth sciences: a tutorial, *Int. J. Geophys.*, 2012, 286107, doi:10.1155/2012/286107, 2012. 2566, 2578, 2640, 2646
- Jouniaux, L. and Pozzi, J.-P.: Permeability dependence of streaming potential in rocks for various fluid conductivity, *Geophys. Res. Lett.*, 22, 485–488, 1995. 2579, 2582
- 15 Jouniaux, L. and Pozzi, J.-P.: Laboratory measurements anomalous 0.1–0.5 Hz streaming potential under geochemical changes: implications for electrotelluric precursors to earthquakes, *J. Geophys. Res.*, 102, 15335–15343, 1997. 2646
- Jouniaux, L., Lallemand, S., and Pozzi, J.: Changes in the permeability, streaming potential and resistivity of a claystone from the Nankai prism under stress, *Geophys. Res. Lett.*, 21, 149–152, 1994. 2579
- 20 Jouniaux, L., Pozzi, J.-P., Berthier, J., and Massé, P.: Detection of fluid flow variations at the Nankai Trough by electric and magnetic measurements in boreholes or at the seafloor, *J. Geophys. Res.*, 104, 29293–29309, 1999. 2616
- Jouniaux, L., Bernard, M.-L., Zamora, M., and Pozzi, J.-P.: Streaming potential in volcanic rocks from Mount Peleé, *J. Geophys. Res.*, 105, 8391–8401, 2000. 2579
- 25 Jouniaux, L., Maineuil, A., Naudet, V., Pessel, M., and Sailhac, P.: Review of self-potential methods in Hydrogeophysics, *C. R. Geosci.*, 341, 928–936, doi:10.1016/j.crte.2009.08.008, 2009. 2565
- Kepic, A. and Rosid, M.: Enhancing the seismoelectric method via a virtual shot gather, 74th SEG Technical Program Expanded Abstracts, Denver, October, 1337–1340, doi:10.1190/1.2428267, 2004. 2599, 2601
- 30

2628

- Kröger, B., Yaramanci, U., and Kemna, A.: Numerical analysis of seismoelectric wave propagation in spatially confined geological units, *Geophys. Prospect.*, 62, 133–147, doi:10.1111/1365-2478.12020, 2014. 2592, 2650
- Kulesa, B., Murray, T., and Rippin, D.: Active seismoelectric exploration of glaciers, *Geophys. Res. Lett.*, 33, L07503, doi:10.1029/2006GL025758, 2006. 2604
- Li, S., Pengra, D., and Wong, P.: Onsager's reciprocal relation and the hydraulic permeability of porous media, *Phys. Rev. E*, 51, 5748–5751, 1995. 2646
- Liu, Z., Yuan, L., Zhang, X., Liu, Z., and Wu, H.: A laboratory seismoelectric measurement for the permafrost model with a frozen–unfrozen interface, *Geophys. Res. Lett.*, 35, L21404, doi:10.1029/2008GL035724, 2008. 2614
- Long, L. T. and Rivers, W. K.: Field measurement of the electroseismic response, *Geophysics*, 40, 233–245, 1975. 2567
- Lorne, B., Perrier, F., and Avouac, J.-P.: Streaming potential measurements. 1. Properties of the electrical double layer from crushed rock samples, *J. Geophys. Res.*, 104, 17857–17877, 1999. 2579, 2646
- Mahardika, H., Revil, A., and Jardani, A.: Waveform joint inversion of seismograms and electrograms for moment tensor characterization of fracking events, *Geophysics*, 77, ID23–ID39, 2012. 2596
- Maineult, A., Jouniaux, L., and Bernabé, Y.: Influence of the mineralogical composition on the self-potential response to advection of KCl concentration fronts through sand, *Geophys. Res. Lett.*, 33, L24311, doi:10.1029/2006GL028048, 2006. 2579
- Markov, M. and Verzhbitskiy, V.: Simulation of the electroseismic effect produced by an acoustic multipole source in a fluid-filled borehole, *SPWLA 45th Annual Logging Symposium, Society of Petrophysicists and Well-Log Analysts (Pubs)*, 6–9 June, Noordwijk, 1–11, 2004. 2593
- Markov, M. and Verzhbitskiy, V.: Electroseismic waves from acoustic source in a fluid-filled borehole, in: *Poromechanics II Biot Centennial (1905–2005)*, edited by: Abousleiman, Y. N., Cheng, A. I. D., and Ulm, F. J., A. A. Balkema, Taylor and Francis Group, London, UK, 283–288, 2005. 2593
- Martner, S. T. and Sparks, N. R.: The electroseismic effect, *Geophysics*, 24, 297–308, 1959. 2567, 2601, 2602, 2605
- McBain, J., Peaker, C., and King, A.: Absolute measurements of the surface conductivity near the boundary of optically polished glass and solutions of potassium chloride, *J. Am. Chem. Soc.*, 51, 3294–3312, 1929. 2567

2629

- Migunov, N. and Kokorev, A.: Dynamic properties of the seismoelectric effect of water-saturated rocks, *Izvestiya, Earth Physics*, 13, 443–445, 1977. 2568, 2609, 2610, 2611, 2616
- Mikhailov, O. V., Haartsen, M. W., and Toksöz, M. N.: Electroseismic investigation of the shallow subsurface: field measurements and numerical modeling, *Geophysics*, 62, 97–105, 1997. 2589, 2603
- Mikhailov, O. V., Queen, J., and Toksöz, M. N.: Using borehole electroseismic measurements to detect and characterize fractured (permeable) zones, *Geophysics*, 65, 1098–1112, 2000. 2565, 2594
- Miller, D.: Thermodynamics of irreversible processes, The experimental verification of Onsager reciprocal relations, *Chem. Rev.*, 60, 15–37, 1960. 2569
- Morgan, F. D., Williams, E. R., and Madden, T. R.: Streaming potential properties of westerly granite with applications, *J. Geophys. Res.*, 94, 12449–12461, 1989. 2583
- Mualem, Y.: A new model for predicting the hydraulic conductivity of unsaturated porous media, *Water Resour. Res.*, 12, 513–522, 1976. 2637
- Neev, J. and Yeatts, F. R.: Electrokinetic effects in fluid-saturated poroelastic media, *Phys. Rev. B*, 40, 9135–9141, 1989. 2568
- Neishtadt, N. M., Eppelbaum, L. V., and Levitski, A. G.: Case History. Application of piezoelectric and seismoelectrokinetic phenomena in exploration geophysics: review of Russian and Israeli experiences, *Geophysics*, 71, B41–B53, 2006. 2566
- Onsager, L.: Reciprocal relations in irreversible processes: I, *Phys. Rev.*, 37, 405–426, 1931. 2568, 2569
- Overbeek, J. T. G.: Electrochemistry of the double layer, in: *Colloid Science, Irreversible Systems*, edited by: Kruyt, H. R., Elsevier, Amsterdam, 115–193, 1952. 2565
- Packard, R. G.: Streaming potentials across capillaries for sinusoidal pressure, *J. Chem. Phys.*, 1, 303–307, 1953. 2571, 2572
- Pain, C., Saunders, J. H., Worthington, M. H., Singer, J. M., Stuart-Bruges, C. W., Mason, G., and Goddard, A.: A mixed finite-element method for solving the poroelastic Biot equations with electrokinetic coupling, *Geophys. J. Int.*, 160, 592–608, 2005. 2593
- Parkhomenko, E. and Gaskarov, I.: Borehole and laboratory studies of the seismoelectric effect of the second kind in rocks, *Izv. Akad. Sci. USSR, Physics Solid Earth*, 9, 663–666, 1971. 2568, 2612
- Parkhomenko, E. and Topchyan, K.: Influence of high-conducting component on the magnitude of seismoelectric effect, *Physics of the Solid Earth*, 30, 727–732, 1995. 2610

2630

- Parkhomenko, I. and Tsze-San, C.: A study of the influence of moisture on the magnitude of the seismoelectric effect in sedimentary rocks by a laboratory method, *Bull. (Izv.) Acad. Sci., USSR, Geophys. Ser.*, 115–118, 1964. 2568, 2612
- Parks, G.: The isoelectric points of solid oxides, solid hydroxides, and aqueous hydroxocomplex, *Chem. Rev.*, 65, 177–198, 1965. 2579
- Paterson, M.: The equivalent channel model for permeability and resistivity in fluid-saturated rock – a re-appraisal, *Mech. Mater.*, 2, 345–352, 1983. 2581
- Pengra, D. B., Li, S. X., and Wong, P.-Z.: Determination of rock properties by low frequency AC electrokinetics, *J. Geophys. Res.*, 104, 29485–29508, 1999. 2646
- Perrier, F. and Froidefond, T.: Electrical conductivity and streaming potential coefficient in a moderately alkaline lava series, *Earth Planet. Sc. Lett.*, 210, 351–363, doi:10.1016/S0012-821X(03)00105-5, 2003. 2646
- Perrier, F. and Morat, P.: Characterization of electrical daily variations induced by capillary flow in the non-saturated zone, *Pure Appl. Geophys.*, 157, 785–810, 2000. 2585, 2637
- Pozzi, J.-P. and Jouniaux, L.: Electrical effects of fluid circulation in sediments and seismic prediction, *C. R. Acad. Sci. Paris, serie II*, 318, 73–77, 1994. 2582
- Pride, S.: Governing equations for the coupled electromagnetics and acoustics of porous media, *Phys. Rev. B*, 50, 15678–15695, 1994. 2568, 2569, 2570, 2616
- Pride, S. and Garambois, S.: Electro seismic wave theory of Frenkel and more recent developments, *J. Eng. Mech.-ASCE*, 131, 697–706, 2005. 2590, 2591, 2648
- Pride, S. and Haartsen, M. W.: Electro seismic wave properties, *J. Acoust. Soc. Am.*, 100, 1301–1315, 1996. 2568, 2575, 2589
- Pride, S. and Morgan, F. D.: Electrokinetic dissipation induced by seismic waves, *Geophysics*, 56, 914–925, 1991. 2580
- Quincke, G.: Über die Fortführung materieller Teilchen durch stromende Elektrizität, *Annalen der Physik und Chemie* 113, 513–598, 1861. 2567
- Ren, H., Huang, Q., and Chen, X.: A new numerical technique for simulating the coupled seismic and electromagnetic waves in layered porous media, *Earthquake Science*, 23, 167–176, 2010. 2591
- Ren, H., Chen, X., and Huang, Q.: Numerical simulation of coseismic electromagnetic fields associated with seismic waves due to finite faulting in porous media, *Geophys. J. Int.*, 188, 925–944, 2012. 2592

2631

- Reppert, P. and Morgan, F.: Temperature-dependent streaming potentials: 1. Theory, *J. Geophys. Res.*, 108, 2546, doi:10.1029/2002JB001754, 2003a. 2583
- Reppert, P. and Morgan, F.: Temperature-dependent streaming potentials: 2. Laboratory, *J. Geophys. Res.*, 108, 2547, doi:10.1029/2002JB001755, 2003b. 2584, 2585
- Reppert, P. M., Morgan, F. D., Lesmes, D. P., and Jouniaux, L.: Frequency-dependent streaming potentials, *J. Colloid Interf. Sci.*, 234, 194–203, doi:10.1006/jcis.2000.7294, 2001. 2570, 2571, 2572, 2642
- Reuss, F.: Sur un nouvel effet de l'électricité galvanique, *Mémoires de la société impériale des naturalistes de Moscou*, 2, 326–337, 1809. 2567
- Revil, A. and Cerepi, A.: Streaming potentials in two-phase flow conditions, *Geophys. Res. Lett.*, 31, L11605, doi:10.1029/2004GL020140, 2004. 2587
- Revil, A. and Glover, P.: Nature of surface electrical conductivity in natural sands, sandstones, and clays, *Geophys. Res. Lett.*, 25, 691–694, 1998. 2582
- Revil, A., Linde, N., Cerepi, A., Jougnot, D., Matthäi, S., and Finsterle, S.: Electrokinetic coupling in unsaturated porous media, *J. Colloid Interf. Sci.*, 313, 315–327, 2007. 2586, 2587, 2645
- Russell, R. D., Butler, K. E., Kepic, A. W., and Maxwell, M.: Seismoelectric exploration, *Leading Edge*, 16, 1611–1615, 1997. 2566, 2567, 2605
- Rutgers, A.: Streaming effects and surface conduction. Streaming potentials and surface conductance, *T. Faraday Soc.*, 35, 69–80, doi:10.1039/TF9403500069, 1940. 2567, 2582
- Santos, J., Zyserman, F., and Gauzellino, P.: Numerical electro seismic modeling: a finite element approach, *Appl. Math. Comput.*, 218, 6351–6374, 2012. 2591
- Santos, J. E.: Finite element approximation of coupled seismic and electromagnetic waves in fluid-saturated poroviscoelastic media, *Numer. Meth. Part. D. E.*, 27, 351–386, 2009. 2591
- Schakel, M. and Smeulders, D.: Seismoelectric reflection and transmission at a fluid/porous-medium interface, *J. Acoust. Soc. Am.*, 127, 13–21, 2010. 2588
- Schakel, M., Smeulders, D., Slob, E., and Heller, H.: Seismoelectric interface response: experimental results and forward model, *Geophysics*, 76, N29–N36, doi:10.1190/1.3592984, 2011. 2610, 2615
- Schakel, M., Smeulders, D., Slob, E., and Heller, H.: Seismoelectric fluid/porous-medium interface response model and measurements, *Transport Porous Med.*, 93, 271–282, doi:10.1007/s11242-011-9869-8, 2012. 2610
- Schoemaker, F., Smeulders, D., and Slob, E.: Simultaneous determination of dynamic permeability and streaming potential, *SEG expanded abstracts*, 26, 1555–1559, 2007. 2571

2632

- Schoemaker, F., Smeulders, D., and Slob, E.: Electrokinetic effect: theory and measurement, SEG Technical Program Expanded Abstracts, 9–14 November, Las Vegas, 1645–1649, 2008. 2571, 2610, 2611
- Sears, A. and Groves, J.: The use of oscillating laminar flow streaming potential measurements to determine the zeta potential of a capillary surface, *J. Colloid Interf. Sci.*, 65, 479–482, 1978. 2571
- Sénéchal, P., Garambois, S., and Bordes, C.: Feasibility of acoustic imaging for in-situ characterization of subsurface soil injected with fresh mortar, *J. Appl. Geophys.*, 72, 184–193, 2010. 2613
- Singarimbun, A., Srigutomo, W., Fauzi, U., and Sunarya, A.: An application of numerical simulation in a seismoelectric phenomena by using transfer function, in: *Proceedings of the Third Asian Physics Symposium APS*, 22–23 July, Bandung, 189–193, 2009. 2591
- Singer, J., Saunders, J., Holloway, L., Stoll, J., Pain, C., Stuart-Bruges, W., and Mason, G.: Electrokinetic logging has the potential to measure the permeability, *Society of Petrophysicists and Well Log Analysts*, 46th Annual Logging Symposium, 26–29 June New Orleans, 2005. 2619, 2662
- Smeulders, D., Eggels, R., and van Dongen, M.: Dynamic permeability: reformulation of theory and new experimental and numerical data, *J. Fluid Mech.*, 245, 211–227, 1992. 2569
- Smeulders, D., Grobbe, N., Heller, H., and Schakel, M.: Seismoelectric conversion for the detection of porous medium interfaces between wetting and nonwetting fluids, *Vadose Zone J.*, 13, doi:10.2136/vzj2013.06.0106, 2014. 2615
- Sposito, G.: *The Chemistry of Soils*, Oxford University, Oxford, 1989. 2579
- Stern, O.: Zur Theorie der electrolytischen Doppelschicht, *Z. Elektrochem.*, 30, 508–516, 1924. 2578
- Strahser, M., Jouniaux, L., Sailhac, P., Matthey, P.-D., and Zillmer, M.: Dependence of seismoelectric amplitudes on water-content, *Geophys. J. Int.*, 187, 1378–1392, 2011. 2565, 2601, 2608
- Strahser, M. H. P., Rabbel, W., and Schildknecht, F.: Polarisation and slowness of seismoelectric signals: a case study, *Near Surf. Geophys.*, 5, 97–114, 2007. 2565, 2599, 2604
- Szarka, L.: Geophysical aspects of man-made electromagnetic noise in the earth – a review, *Surv. Geophys.*, 9, 287–318, 1987. 2597
- Tardif, E., Glover, P., and Ruel, J.: Frequency-dependent streaming potential of Ottawa sand, *J. Geophys. Res.*, 116, B04206, doi:10.1029/2010JB008053, 2011. 2571

2633

- Thompson, A., Hornbostel, S., Burns, J., Murray, T., Raschke, R., Wride, J., McCammon, P., Sumner, J., Haake, G., Bixby, M., Ross, W., White, B., Zhou, M., and Peczak, P.: Field tests of electroseismic hydrocarbon detection, SEG Technical Program Expanded Abstracts, 565–568, 2005. 2564, 2565, 2607, 2608, 2639
- Thompson, A., Sumner, J., and Hornbostel, S.: Electromagnetic-to-seismic conversion: a new direct hydrocarbon indicator, *Leading Edge*, 26, 428–435, 2007. 2564, 2600, 2607, 2608, 2638
- Thompson, A. H. and Gist, G. A.: Geophysical applications of electrokinetic conversion, *Leading Edge*, 12, 1169–1173, 1993. 2568, 2573, 2574, 2597, 2601, 2606
- Thompson, R. R.: A note on the seismic-electric effect, *Geophysics*, 4, 102–103, 1939. 2567
- Thyssen, S. V., Hummel, J., and Rülke, O.: Die Ursachen des seismisch-elektrischen Effektes, *Z. Geophys.*, 13, 112–119, 1937. 2567
- Tosha, T., Matsushima, N., and Ishido, T.: Zeta potential measured for an intact granite sample at temperatures to 200°C, *Geophys. Res. Lett.*, 30, 1295, doi:10.1029/2002GL016608, 2003. 2584, 2585
- Urban, F. and White, H.: Application of the double layer theory of Otto Stern. I, *J. Phys. Chem.*, 36, 3157–3161, 1932. 2567
- Valuri, J., Dean, T., and Dupuis, J.: Seismoelectric acquisition in an arid environment, 22nd International Geophysical Conference and Exhibition, 26–29 February 2012, Brisbane, 2012. 2601
- VanCappellen, P., Charlet, L., Stumm, W., and Wersin, P.: A surface complexation model of the carbonate mineral-aqueous solution interface, *Geochim. Cosmochim. Acta*, 57, 3505–3518, 1993. 2580
- Vinogradov, J., Jaafar, M., and Jackson, M. D.: Measurement of streaming potential coupling coefficient in sandstones saturated with natural and artificial brines at high salinity, *J. Geophys. Res.*, 115, B12204, doi:10.1029/2010JB007593, 2010. 2579
- von Helmholtz, H.: Studien über elektrische Grenzschichten, *Annalen der Physik und Chemie*, Neue Folge, 7, 337–382, 1879. 2567
- Walker, E. and Glover, P. W. J.: Permeability models of porous media: characteristic length scales, scaling constants and time-dependent electrokinetic coupling, *Geophysics*, 75, E235–E246, doi:10.1190/1.3006561, 2010. 2572

2634

- Wang, J. and Hu, H.: The determination of electrokinetic coupling coefficient and zeta potential of rock samples by electrokinetic measurements, *Adv. Mat. Res.*, 516–517, 1870–1873, 2012. 2582
- Wang, Z., Hu, H., and Guan, W.: Three-dimensional finite-difference time-domain computation of the seismoelectric field generated by a slipping fault, in: *Poromechanics V: Proceedings of the Fifth Biot Conference on Poromechanics*, edited by: Hellmich, C., Pichler, B., and Adam, D., 2032–2041, 10–12 July, Vienna, 2013. 2596
- Warden, S., Garambois, S., Sailhac, P., Jouniaux, L., and Bano, M.: Curvelet-based seismoelectric data processing, *Geophys. J. Int.*, 190, 1533–1550, doi:10.1111/j.1365-246X.2012.05587.x, 2012. 2600
- Warden, S., Garambois, S., Jouniaux, L., Brito, D., Sailhac, P., and Bordes, C.: Seismoelectric wave propagation numerical modeling in partially saturated materials, *Geophys. J. Int.*, 194, 1498–1513, doi:10.1093/gji/ggt198, 2013. 2577, 2595, 2651
- White, B. and Zhou, M.: Electrostatic prospecting in layered media, *SIAM J. Appl. Math.*, 67, 69–98, 2006. 2588
- White, B. S.: Asymptotic theory of electrostatic prospecting, *SIAM J. Appl. Math.*, 65, 1443–1462, 2005. 2588
- White, H., Urban, F., and Monaghan, B.: The magnitude of surface conductivity at aqueous-glass interfaces, *J. Phys. Chem.*, 45, 560–570, 1941. 2567
- Wiedemann, G.: Über die Bewegung von Flüssigkeiten im Kreise der geschlossenen galvanischen Saule, *Annalen der Physik und Chemie*, 87, 321–352, 1852. 2567
- Xia, J. and Miler, D.: Design of a hum filter for suppressing power-noise in seismic data, *J. Environ. Eng. Geoph.*, 5, 31–38, 2000. 2597
- Yeh, C., Chen, S., Teng, T., and Lee, Y.: On formulation of a transition matrix for electroporoelastic medium and application to analysis of scattered electrostatic wave, *J. Acoust. Soc. Am.*, 120, 3672, 2006. 2591
- Zhan, X., Chi, S., and Toksöz, M.: Simulation of the converted electric field during multipole logging while drilling (LWD), 76th SEG Annual International Meeting, Expanded Abstracts, New Orleans, 1–6 October, 25, 446–450, 2006a. 2618
- Zhan, X., Zhu, Z., Chi, S., Rao, R., Burns, D., and Toksöz, M.: Elimination of LWD (Logging While Drilling) Tool Modes, Technical Report MIT, Cambridge, United States, 1–32, 2006b. 2593, 2618

- Zhang, Y., Xiao, L., Chu, Z., and Li, J.: The converted electromagnetic wave characteristics of seismoelectric conversion effect in borehole, *Chinese J. Geophys.*, 48, 501–508, 2005. 2617
- Zhou, J., Cui, Z., and Lü, W.: Seismoelectric waves in a borehole excited by an external explosive source, *Chinese Phys. B*, 23, 014301-1–014301-6, 2014. 2593
- Zhu, Z. and Toksöz, M.: Experimental measurements of the streaming potential and seismoelectric conversion in Berea sandstone, *Geophys. Prospect.*, 61, 688–700, doi:10.1111/j.1365-2478.2012.01110, 2013. 2611
- Zhu, Z. and Toksöz, M. N.: Crosshole seismoelectric measurements in borehole models with fractures, *Geophysics*, 68, 1519–1524, 2003. 2617, 2618, 2660, 2661
- Zhu, Z., Haartsen, M. W., and Toksöz, M. N.: Experimental studies of electrokinetic conversions in fluid-saturated borehole models, *Geophysics*, 64, 1349–1356, 1999. 2617, 2620
- Zhu, Z., Haartsen, M. W., and Toksöz, M. N.: Experimental studies of seismoelectric conversions in fluid-saturated porous media, *J. Geophys. Res.*, 105, 28055–28064, 2000. 2609, 2610, 2612
- Zhu, Z., Toksöz, M., and Burns, D.: Electrostatic and seismoelectric measurements of rock sample in a water tank, *Geophysics*, 73, E153–E164, doi:10.1190/1.2952570, 2008. 2620
- Zyserman, F., Gauzellino, P., and Santos, J.: Finite element modeling of SHTE and PSVTM electrostatics, *J. Appl. Geophys.*, 72, 79–91, doi:10.1016/j.jappgeo.2010.07.004, 2010. 2591
- Zyserman, F., Gauzellino, P., and Santos, J.: Numerical evidence of gas hydrate detection by means of electrostatics, *J. Appl. Geophys.*, 86, 98–108, 2012. 2591, 2649
- Zyserman, F., Jouniaux, L., Warden, S., and Garambois, S.: Borehole seismoelectric logging using a shear-wave source: possible application to CO₂ disposal?, *Int. J. Greenh. Gas Con.*, 33, 82–102, doi:10.1016/j.ijggc.2014.12.009, 2015. 2594

Table 1. Streaming Potential Coefficient behaviours as a function of water-saturation. The effective saturation S_e is defined in Eq. (30) in which S_{wr} denotes the residual saturation, n is Archie's saturation exponent, L and λ are the Mualem's parameters in the relative permeability formula Mualem (1976).

Reference	$C_{s0}(S_w)/C_{sat}$
Perrier and Morat (2000)	S_e^2/S_w^n
Guichet et al. (2003)	S_e
Jackson (2010)	$S_e^{(L+2+2/\lambda)}Q_r(S_w)/S_w^n$
Allègre et al. (2012)	$S_e(1 + 32(1 - S_e)^{0.4})$

2637

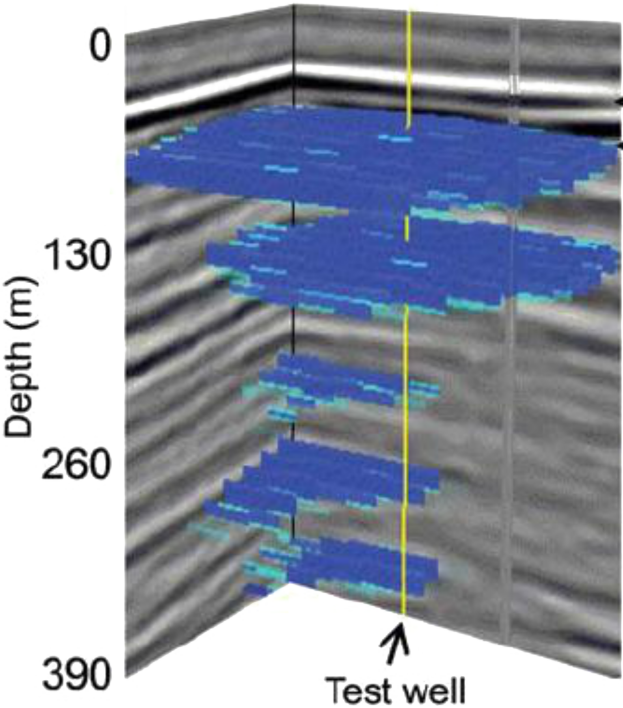


Figure 1. Geometry of a gas reservoir (in blue) deduced from electroseismics (from Thompson et al., 2007).

2638

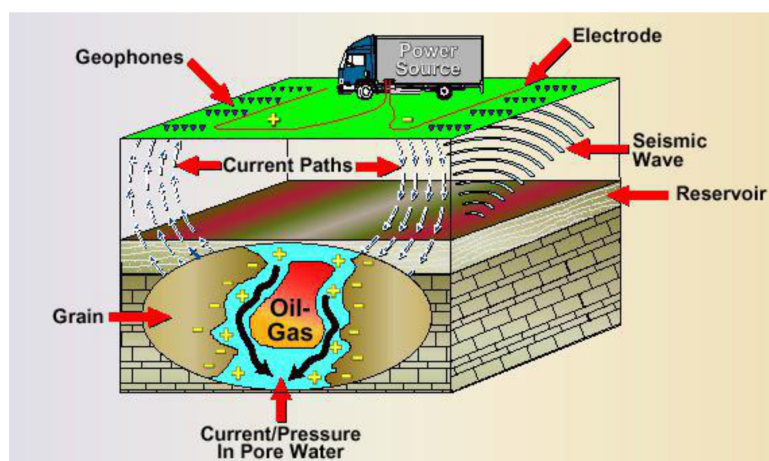


Figure 2. Electroseismics method: an electric current is applied at the surface, and when it encounters a contrast in physical properties it induces a seismic wave which is measured at the surface (from Thompson et al., 2005).

2639

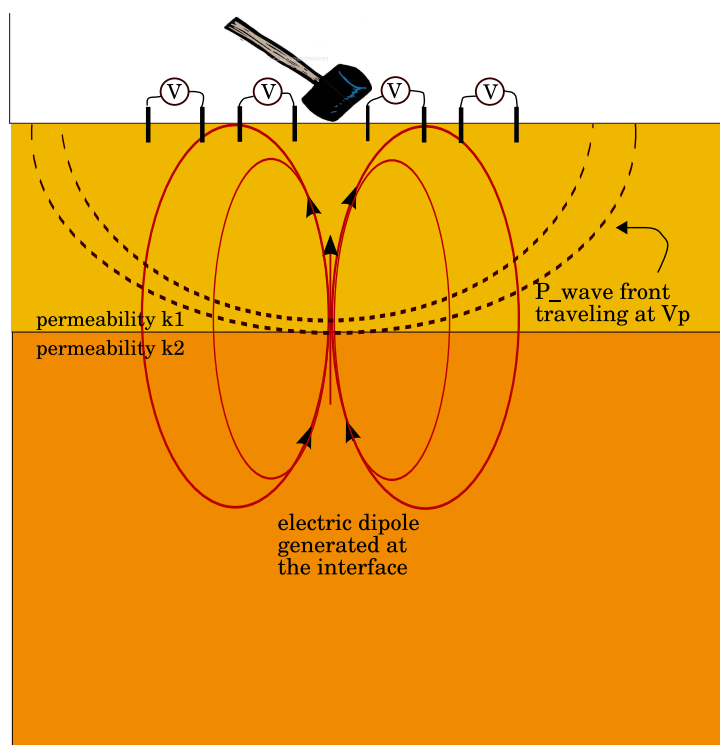


Figure 3. The seismic waves propagates up to the interface where an electric dipole is generated because of the contrast in permeability. This electromagnetic wave can be detected at the surface by measuring the difference of the electrical potential V between electrodes. Picking the time arrival allows to know the depth of the interface (from Jouniaux and Ishido, 2012).

2640

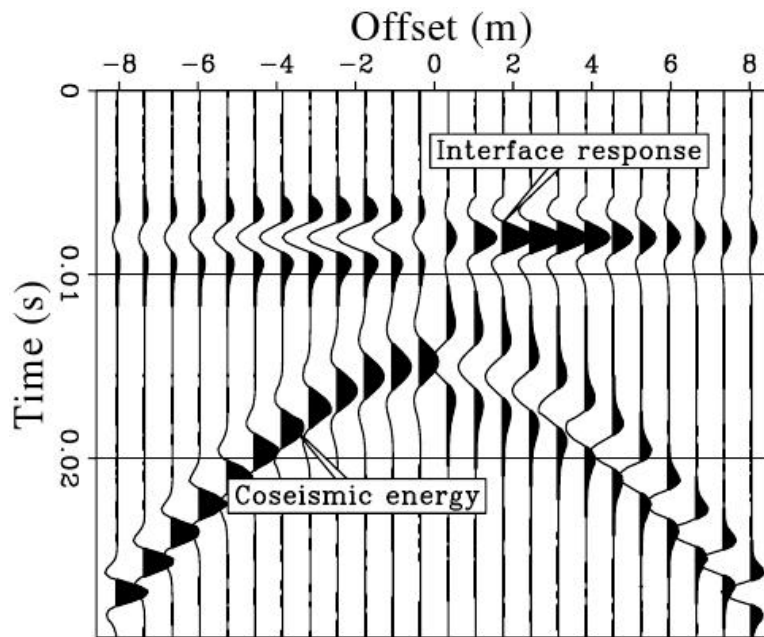


Figure 4. Model of the seismoelectric response to a hammer strike on the surface at position zero (from Haines, 2004). The seismoelectric signal is shown as measured at the surface along a line centered on the seismic source. The interfacial signal is related to a contrast between properties of the media, such as the permeability.

2641

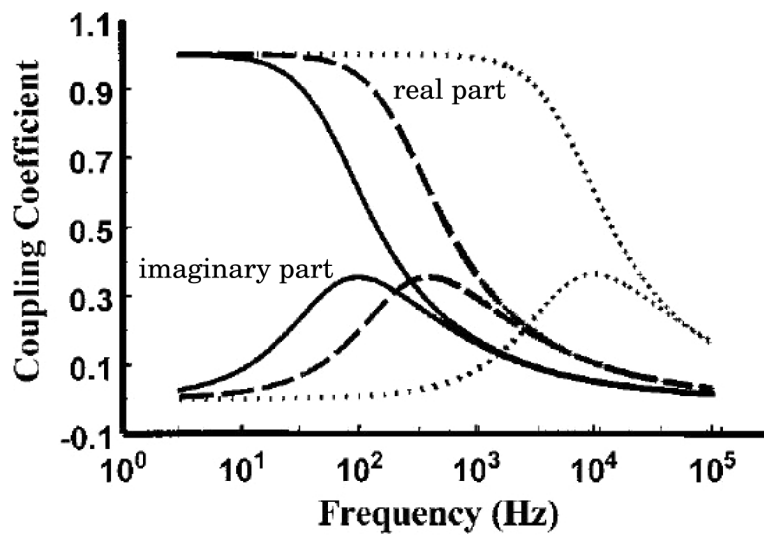


Figure 5. The real and imaginary part of the Packard's model (Eq. 8) calculated by Reppert et al. (2001) for three capillary radii: 100 μm (continuous line), 50 μm (dashed line), 10 μm (point line) (modified from Reppert et al., 2001).

2642

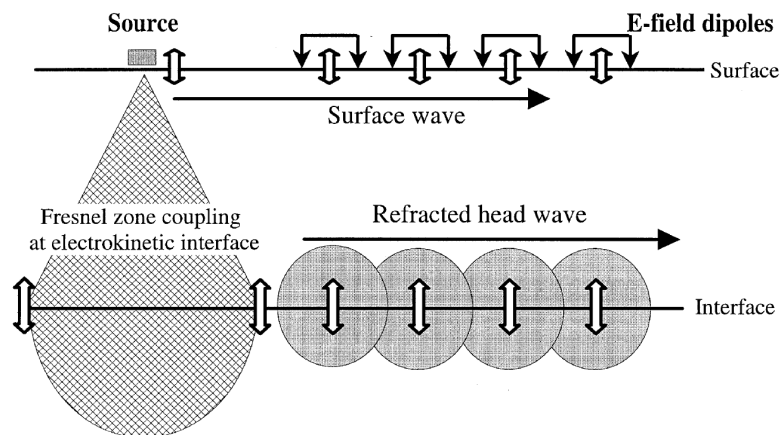


Figure 6. Schematic diagram of three possible mechanisms of electro-seismic coupling due to an acoustic source on the surface (from Beamish, 1999).

2643

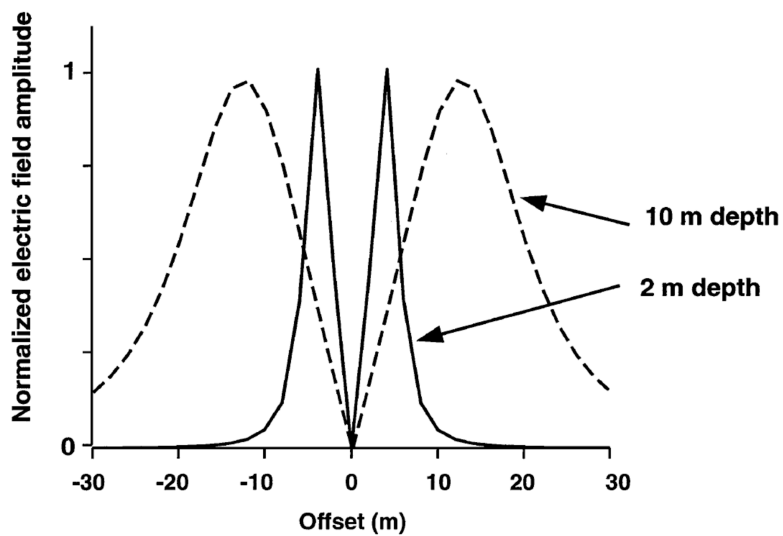


Figure 7. The calculated longitudinal electric field radiated by an arrangement of elementary dipoles at different depths, as a function of the distance to the source (from Garambois and Dietrich, 2001).

2644

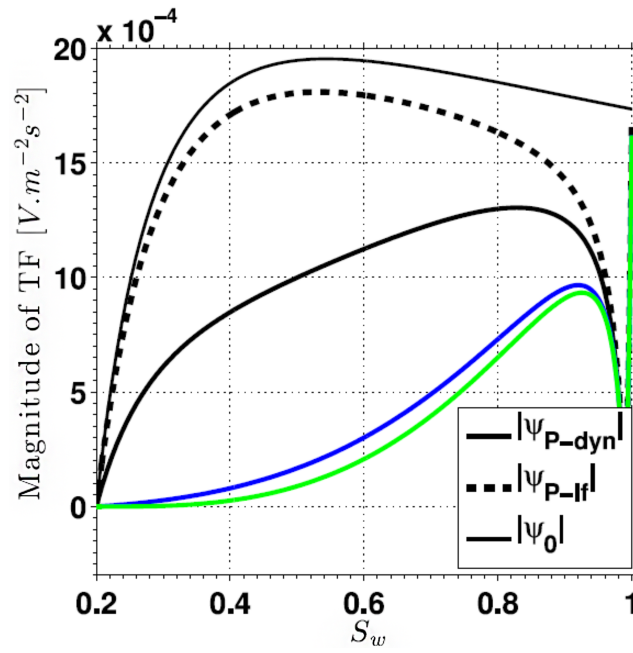


Figure 8. Magnitudes of the P wave dynamic transfer function as a function of the saturation S_w , assuming the Jackson (2010) model for the electrokinetic coefficient, respectively for the P waves dynamic transfer function Ψ_{P-dyn} at $f = 1.5$ kHz, for the P waves low frequency transfer function Ψ_{P-lf} and for the P waves simplified low frequency transfer function Ψ_0 in a partially saturated silica sand (see Eqs. 18 and 19). Magnitude of dynamic transfer functions obtained with the models of Guichet et al. (2003) and Revil et al. (2007) are respectively displayed by blue and green curves (from Bordes et al., 2015).

2645

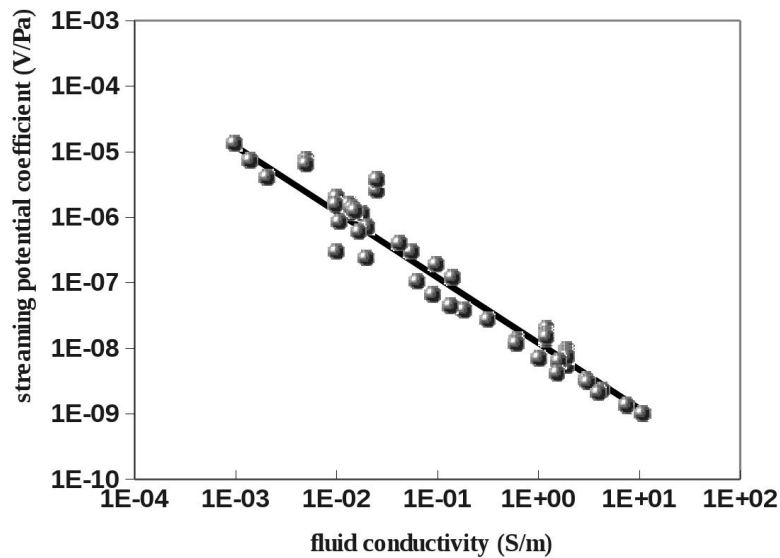


Figure 9. Streaming potential coefficient from data collected (in absolute value) on sands and sandstones at pH 7–8 (when available) from Ahmad (1964); Li et al. (1995); Jouniaux and Pozzi (1997); Lorne et al. (1999); Pengra et al. (1999); Guichet et al. (2003); Perrier and Froidefond (2003); Guichet et al. (2006); Ishido and Mizutani (1981); Jaafar et al. (2009). The regression (black line) leads to $C_{s0} = -1.2 \times 10^{-8} \sigma_f^{-1}$. A zeta potential of -17 mV can be inferred from these collected data (from Jouniaux and Ishido, 2012; Allègre et al., 2010).

2646

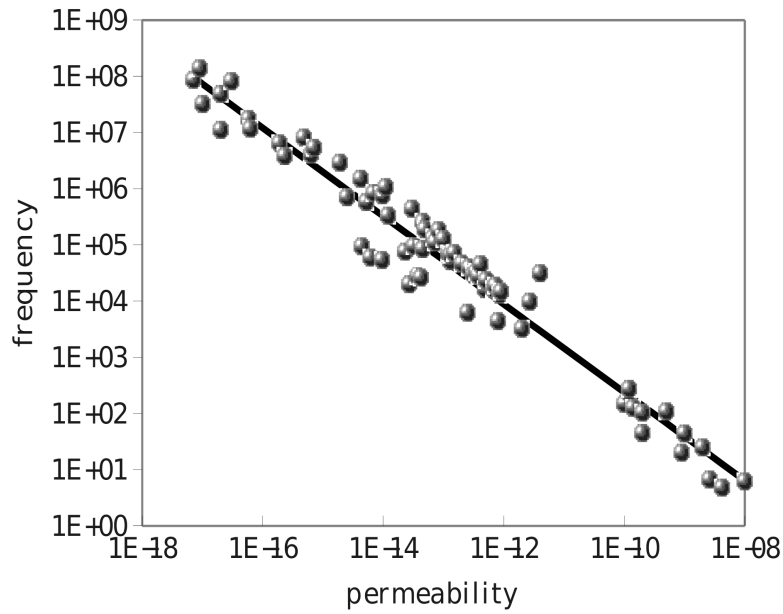


Figure 10. The transition frequency $f_c = \omega_c/2\pi$ (in Hz) predicted using ω_c from Eq. (31) with $\eta = 10^{-3}$ Pa s and $\rho_f = 10^3$ kg m $^{-3}$ as a function of the permeability (in m 2). The transition frequency varies as $\log_{10}(f_c) = -0.78\log_{10}(k) - 5.5$. The parameters of the samples, F and k_0 are measured from different authors on various samples (from Jouniaux and Bordes, 2012).

2647

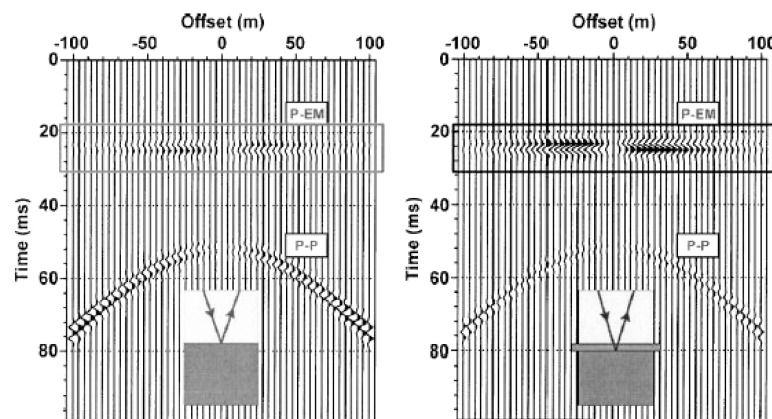


Figure 11. To the left, P_t -EM IR response between two fully saturated porous media with different mechanical properties. To the right, a thin (1 cm) layer of a third material with a lower permeability is introduced between the given media; in this case the converted electric field is roughly ten times larger than in the previous one (from Pride and Garambois, 2005).

2648

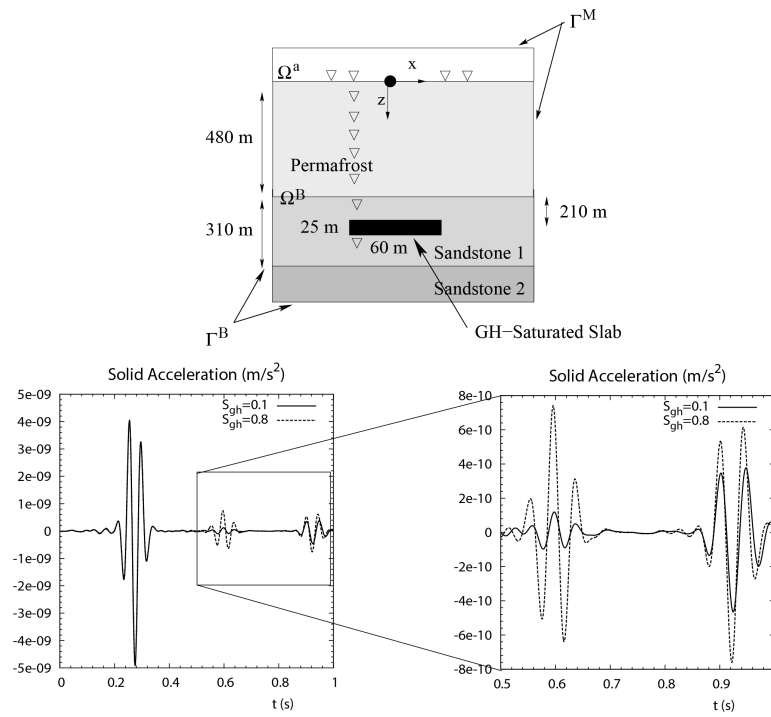


Figure 12. SHTe-mode solid acceleration traces for different gas hydrates reservoir saturations, for the shown model. The first wave train corresponds to the conversion generated at the permafrost base, the second one to the conversions at the slab – top and bottom IR's are indistinguishable one from each other – and finally, the wavetrain arriving at about 0.9 s is the reflection on the slab of the seismic waves originated on the permafrost/sandstone interface (from Zyserman et al., 2012).

2649

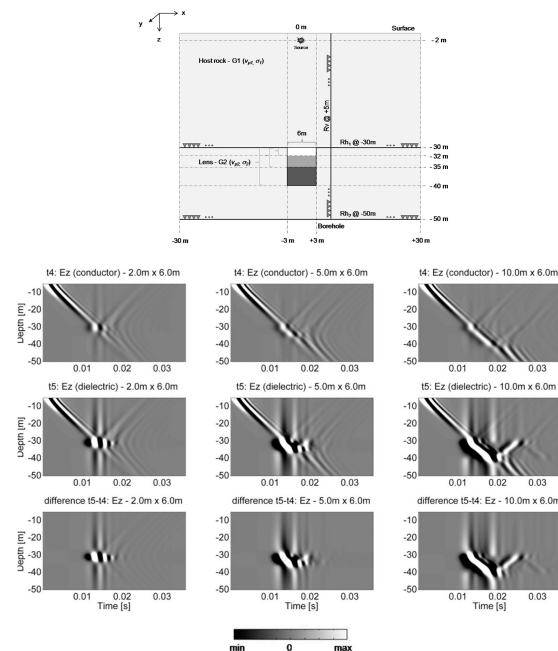


Figure 13. Model and electrograms for the following confined unit geometries: the left column is for 2m x 6m the middle column is for 5m x 6m and the right column is for 10m x 6m. The top row shows the z component of the electric field for a material with electrical conductivity of 0.05 Sm^{-1} , the middle row shows the z component of the electric field for a material with electrical conductivity of 10^{-5} Sm^{-1} . The bottom row shows the calculated differences in the amplitudes for both previous models. Notice that all amplitudes are scaled identically and that the electric conductivity is the only medium parameter with contrasts among different units (from Kröger et al., 2014).

2650

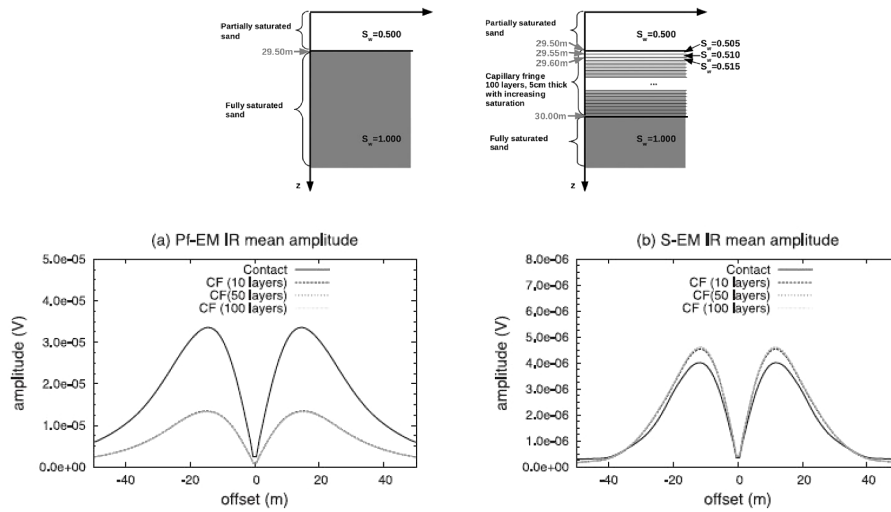


Figure 14. Comparison of the mean amplitudes of the Interface Response induced by compressional waves (bottom left) and shear waves (bottom right), for a sharp saturation transition (top left model) between the two considered regions and for a gradual saturation transition, as given for the capillary fringe shown in the top right model. The S-EM IR response is stronger for the capillary fringe than for the sharp saturation transition, while the P_1 -EM IR response is stronger for the sharp concentration transition than for the capillary fringe (from Warden et al., 2013).

2651

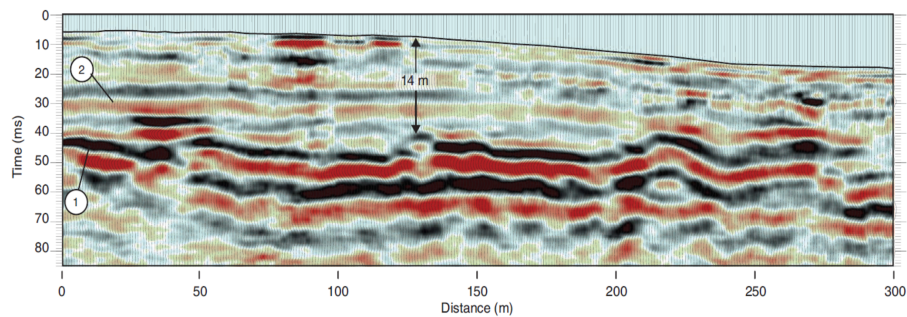


Figure 15. Seismoelectric profile: the event 1 is associated to the water table at 14 m depth; the event 2 is associated to a shallower water-retentive layer not resolved by seismic reflection or refraction (from Dupuis et al., 2007).

2652

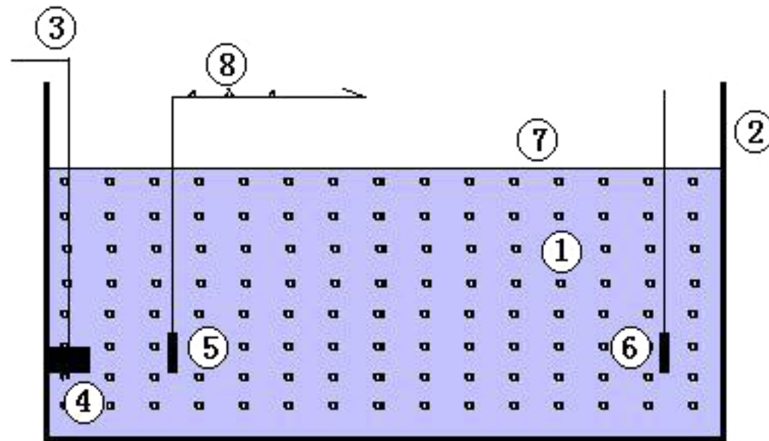


Figure 16. Experimental apparatus. (1) saturated sand, (2) plexiglass box, (3) shielded wire, (4) ultrasonic source; (5) receiver electrode, (6) reference electrode, (7) free surface (air), (8) receiving set-ups (from Chen and Mu, 2005).

2653

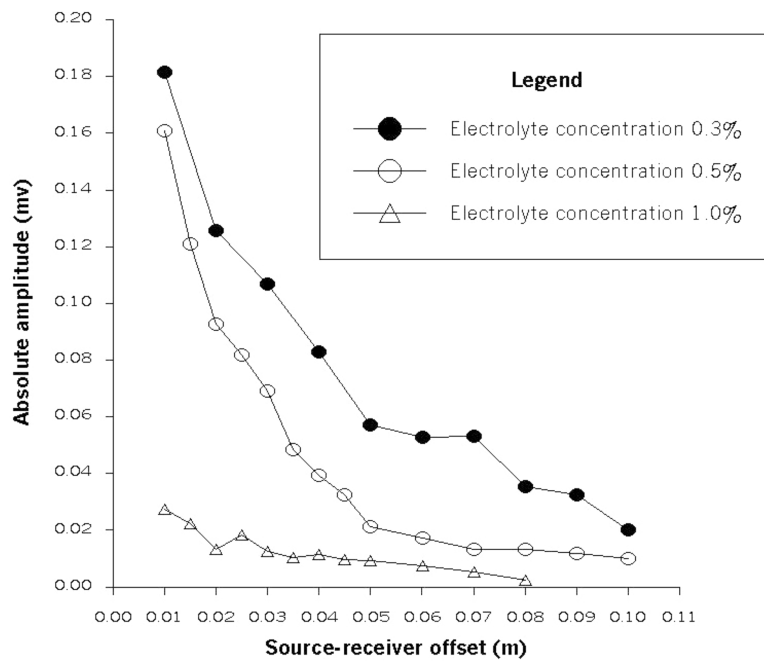


Figure 17. The amplitude of the first kind of seismo-electric conversion as a function of the source-receiver offset. The electrolyte concentration is NaCl concentration (from Chen and Mu, 2005).

2654

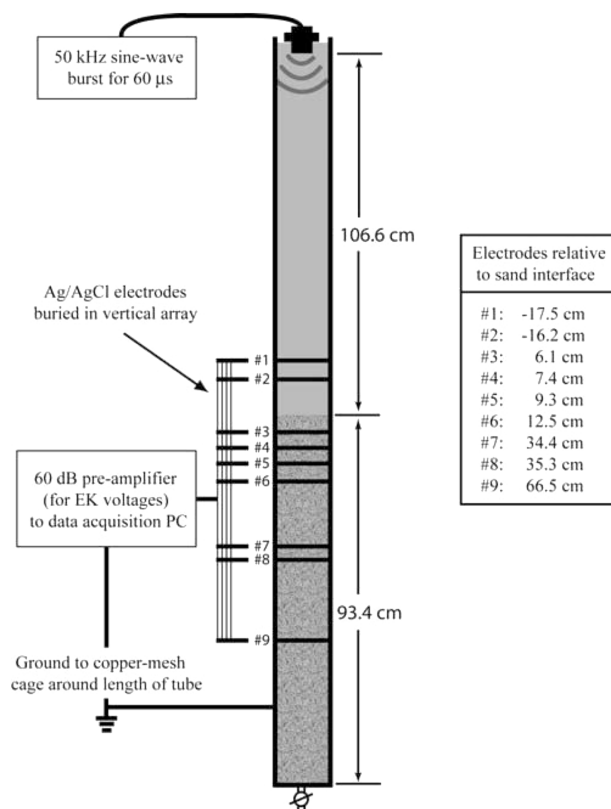


Figure 18. Experimental apparatus with an upper-layer of water above a saturated-sand layer (from Block and Harris, 2006).

2655

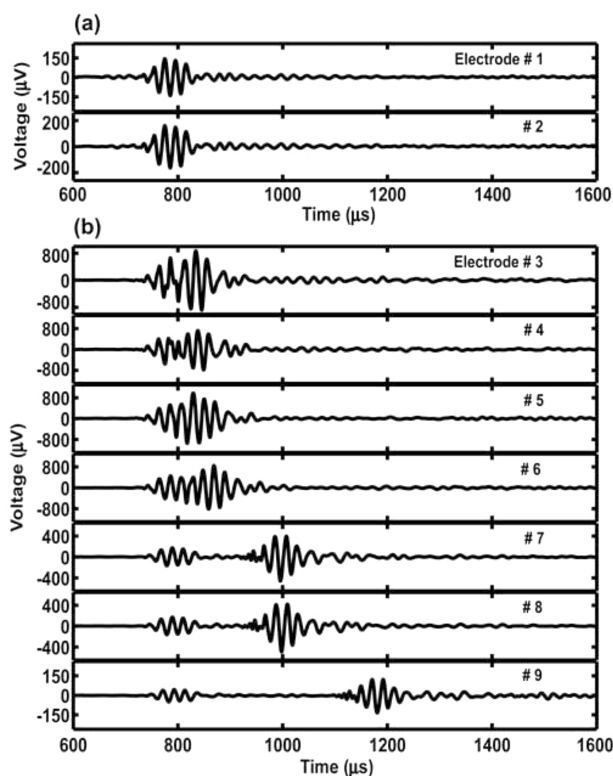


Figure 19. Recording of the electrodes: the simultaneous wave arrival in water and sand is the interfacial response, and the move out signal is related to the transmitted wave. The water conductivity is 0.0076 S m^{-1} (from Block and Harris, 2006).

2656

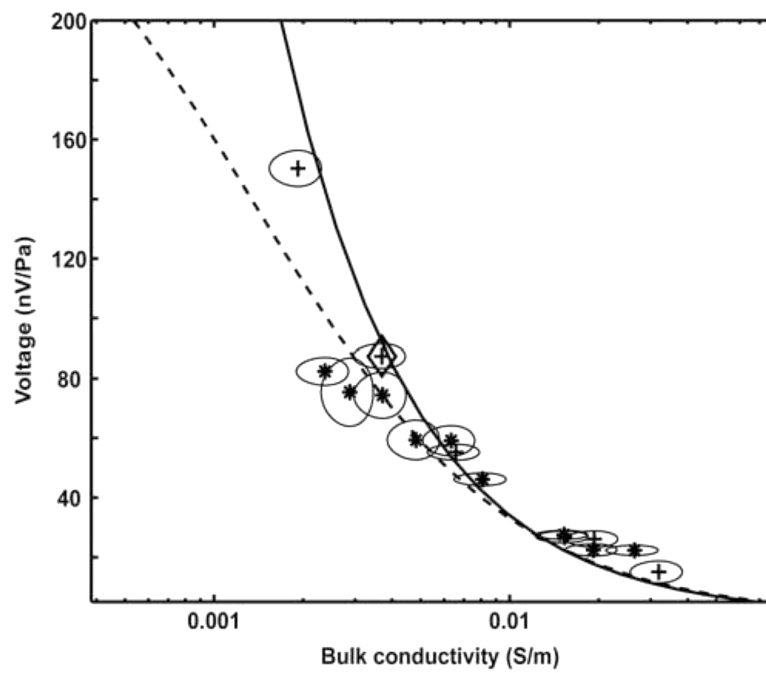


Figure 20. Peaks of the fast wave potentials measured at electrode 8 vs. the bulk conductivity. Measurements are performed on sand and glass microspheres and compared to the theory which predicts that the magnitude of seismoelectric potentials increases as the conductivity is lowered (from Block and Harris, 2006).

2657

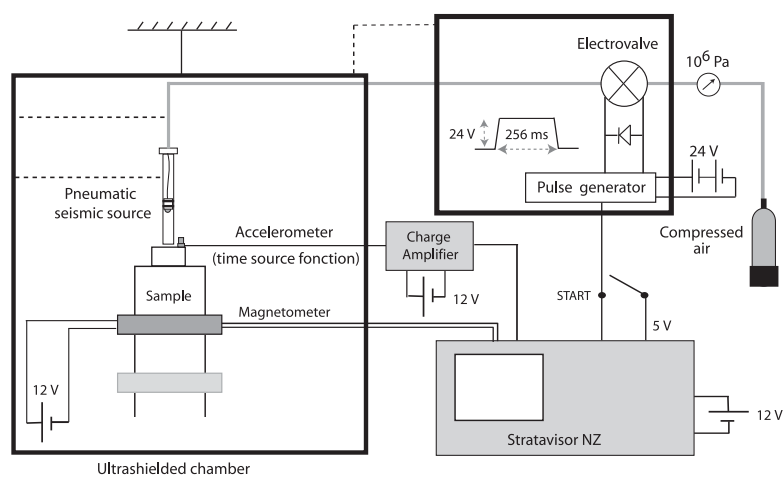


Figure 21. Scheme of the experiment developed in the underground laboratory of Rustrel to measure the magnetic part of the seismo-electromagnetic conversions (from Bordes et al., 2008).

2658

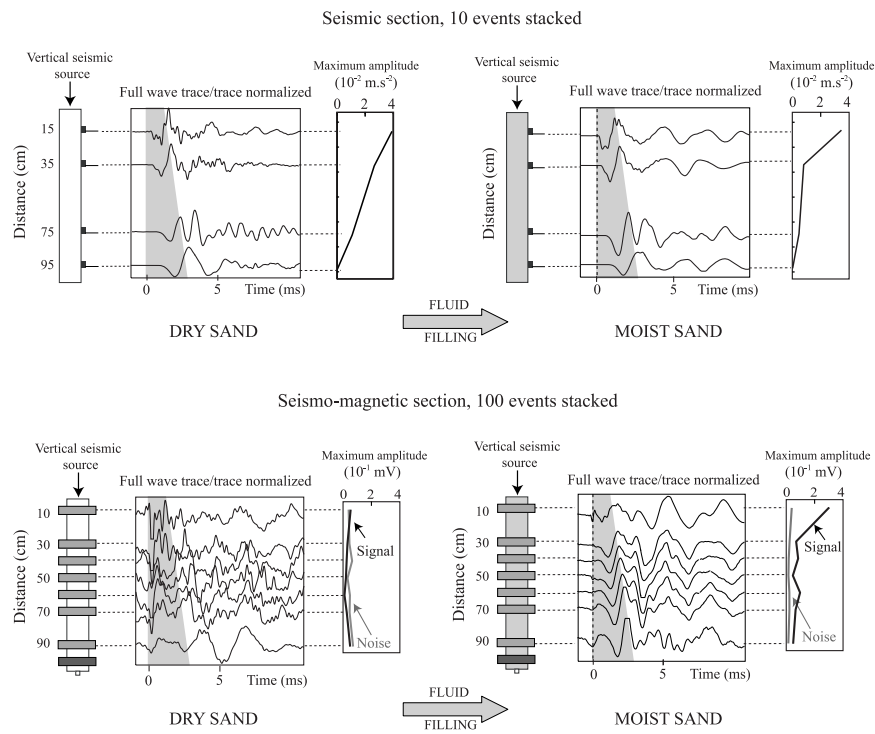


Figure 22. Measurements of the seismic and magnetic field in dry and moist sand showing the evidence of coherent magnetic arrival in the moist sand (from Bordes et al., 2008).

2659

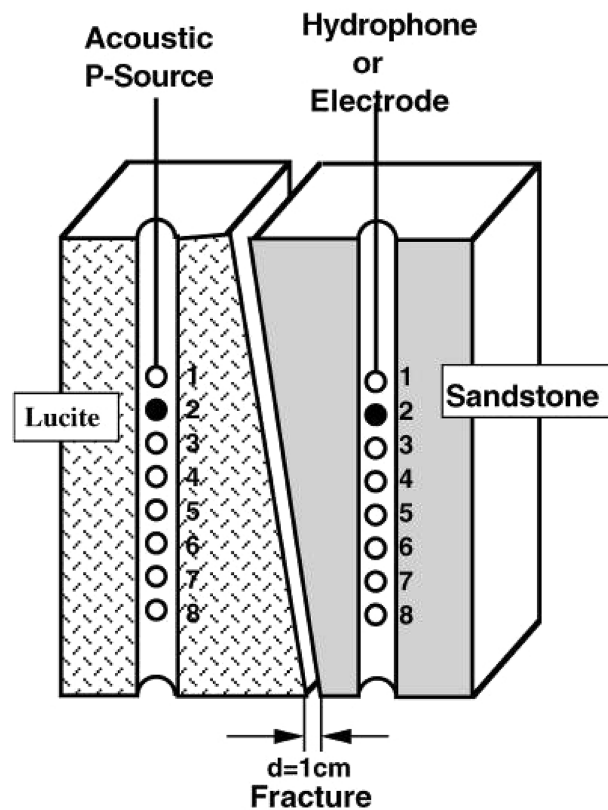


Figure 23. Experimental setup of a crosshole model with an inclined fracture. The angle between the fracture and the horizontal direction is about 70° (from Zhu and Toksöz, 2003).

2660

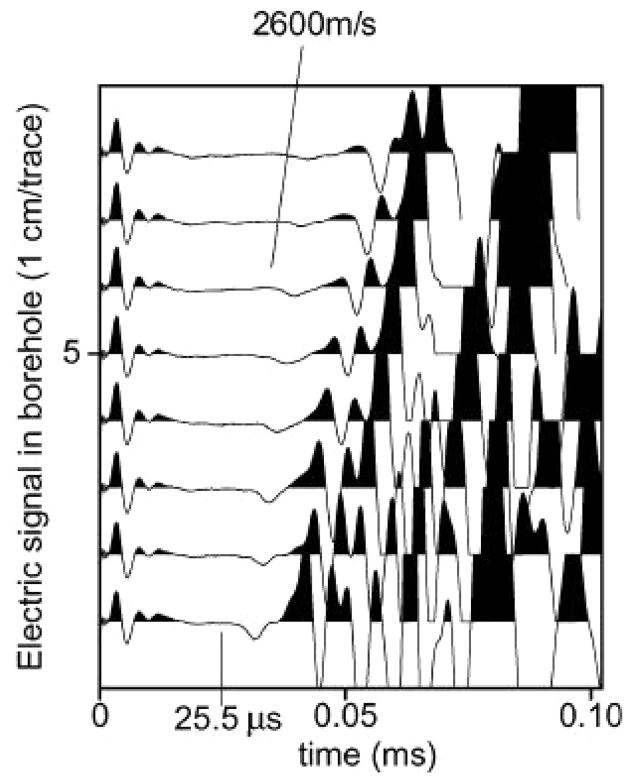


Figure 24. Seismoelectric signals recorded at electrode 2 when the source moves from position 1 to 8. The amplitude is normalized by $14 \mu\text{V}$. The arrival at a velocity 2600 ms^{-1} is the interfacial response of the fracture at the sandstone side (from Zhu and Toksöz, 2003).

2661

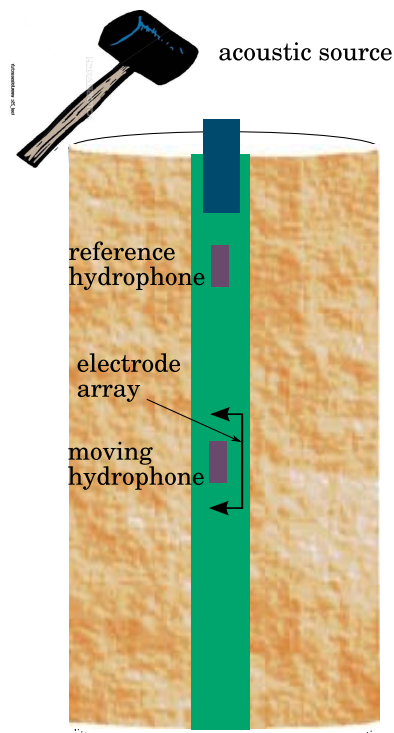


Figure 25. Scheme of the principle of electrokinetic logging to measure the permeability (modified from Singer et al., 2005, in Jouniaux, 2011). The acoustic source induces a Stoneley wave propagation (detected by the hydrophones) leading to an electric field (measured by the electrodes). The experiment is repeated by moving the tool downward.

2662